## ก.3). การนำผลงานวิจัยไปใช้ประโยชน์

- เชิงวิชาการ (มีการพัฒนาการเรียนการสอน/สร้างนักวิจัยใหม่)

<u>ก.3.1 พัฒนาการเรียนการสอน</u> ชุดทดลองในงานวิจัยนี้ ใช้ประกอบการเรียนการสอน ระดับปริญญาโทและปริญญาเอก วิชา Power Electronics Design รหัสวิชา: 225434 ภาควิชาครุศาสตร์ไฟฟ้า คณะครุศาสตร์อุตสาหกรรม มหาวิทยาลัยเทคโนโลยีพระจอมเกล้าพระนครเหนือ



ก.3.2 นักวิจัยที่สำเร็จการศึกษาระดับปริญญาโทจำนวน 1 คนนายสุวัจน์ สิกบุตร

Thesis Title: Control of Renewable Energy: Hybrid System for Grid Independent Applications มหาวิทยาลัยเทคโนโลยีพระจอมเกล้าพระนครเหนือ 2015 หมายเหตุ เป็นที่ปรึกษาร่วม

IEEE TRANSACTIONS ON SUSTAINABLE ENERGY, VOL. 4, NO. 1, JANUARY 2013

## Intelligent Model-Based Control of a Standalone Photovoltaic/Fuel Cell Power Plant With Supercapacitor Energy Storage

Phatiphat Thounthong, Member, IEEE, Arkhom Luksanasakul, Poolsak Koseeyaporn, and Bernard Davat, Member, IEEE

Abstract-A renewable energy hybrid power plant, fed by photovoltaic (PV) and fuel cell (FC) sources with a supercapacitor (SC) storage device and suitable for distributed generation applications, is proposed herein. The PV is used as the primary source; the FC acts as a backup, feeding only the insufficiency power (steady-state) from the PV; and the SC functions as an auxiliary source and a short-term storage system for supplying the deficiency power (transient and steady-state) from the PV and the FC. For high-power applications and optimization in power converters, four-phase parallel converters are implemented for the FC converter, the PV converter, and the SC converter, respectively. A mathematical model (reduced-order model) of the FC, PV, and SC converters is described for the control of the power plant. Using the intelligent fuzzy logic controller based on the flatness property for dc grid voltage regulation, we propose a simple solution to the fast response and stabilization problems in the power system. This is the key innovative contribution of this research paper. The prototype small-scale power plant implemented was composed of a PEMFC system (1.2 kW, 46 A), a PV array (0.8 kW), and an SC module (100 F, 32 V). Experimental results validate the excellent control algorithm during load cycles.

Index Terms-Flatness control, fuel cells, fuzzy control, nonlinear system, photovoltaic, supercapacitor.

## NOMENCLATURE

dc	Direct current.
FC	Fuel cell.
PV	Photovoltaic.
SC	Supercapacitor.

Manuscript received December 06, 2011; revised June 13, 2012; accepted August 15, 2012. Date of publication October 02, 2012; date of current version December 12, 2012. This work was supported in part by the research program in cooperation with the Thai-French Innovation Institute (TFII), King Mongkut's University of Technology North Bangkok (KMUTNB) with Université de Lorraine, and in part by the Thailand Research Fund and Faculty of Technical Education (Research Grant for Mid-Career University Faculty) under

P. Thouthong. A. Luksanasakul, and P. Koseeyaporn are with the Renewable Energy Research Centre (RERC), Department of Teacher Training in Electrical Engineering, Faculty of Technical Education, King Mongkut's University of Technology North Bangkok, Bangkok 10800, Thailand (e-mail: phtt@kmutnb.ac.th; luksanasakul@gmail.com; drpoolsak@gmail.com).

B. Davat is with the Groupe de Recherche en Electrotechnique et Electronique de Nancy, Université de Lorraine, Nancy-Lorraine, France (e-mail: Bernard.Davat@ensem.inpl-nancy.fr).
Color versions of one or more of the figures in this paper are available online

at http://ieeexplore.ieee.org.
Digital Object Identifier 10.1109/TSTE.2012.2214794

CBus Total capacitance at dc bus (F).

 $C_{SC}$ Total capacitance of supercapacitor module (F).

DC bus load current (A). \$Load

Fuel cell current (A). iFC

Fuel cell current reference (set-point) (A). *i*FCREF Solar cell (photovoltaic) current (A). Solar cell current reference (set-point) (A). PVREF

Supercapacitor current (A).

Supercapacitor current reference (set-point) (A). iSCREF

MPPT Maximum power point tracking.

Load power (W). Fuel cell power (W). PFC

Fuel cell output power to dc bus (W).

Fuel cell power reference (set-point) (W). PECREF Maximum fuel cell power (W). PFCMax

Solar cell (photovoltaic) power (W). PPV Solar cell output power to dc-bus (W). Solar cell power reference (set-point) (W). PPVREF

Maximum solar cell power (W). PPVMax Supercapacitor power (W). PSC

Supercapacitor output power to dc-bus (W). PSCo.

Supercapacitor power reference (set-point) (W). PSCREF

Maximum supercapacitor power (W). PSCMax

DC bus voltage (V). v<sub>Bus</sub> Fuel cell voltage (V). VFC

Solar cell (photovoltaic) voltage (V). vPV

Supercapacitor voltage (V).

DC bus energy (J).  $E_{\rm Bus}$ 

DC bus energy reference (set-point) (J). EBusker

Supercapacitor energy (J). Esc

ESCREF Supercapacitor energy reference (set-point) (J). Total energy at dc bus and supercapacitor (J).

1949-3029/\$31.00 © 2012 IEEE

THOUNTHONG et al.: INTELLIGENT MODEL-BASED CONTROL OF A STANDALONE PV/FC POWER PLANT WITH SC ENERGY STORAGE

$r_{\rm FC}$	Equivalent series resistance in fuel cell converter $(\Omega)$ .
$r_{ m PV}$	Equivalent series resistance in solar cell converter $(\Omega)$ .
$r_{\rm SC}$	Equivalent series resistance in supercapacitor converter ( $\Omega$ ).
u	Input variable vector.
x	State-variable vector.
y	Output vector.
$\phi(\cdot), \varphi(\cdot),$ and $\psi(\cdot)$	Smooth mapping functions.

### I. INTRODUCTION

R ENEWABLE energy sources are predicted to become competitive with conventional power generation systems in the near future. Unfortunately, they are not very reliable. For example, the PV source is not available during the night or during cloudy conditions. Other sources such as FCs may be more reliable but have economic issues associated with them. Because of this, two or more renewable energy sources are required to ensure a reliable and cost-effective power solution. Such a combination of different types of energy sources into a system is called a hybrid power system [1].

A combination of PV and FC sources forms a good pair with promising features for distributed generation applications [2]. Obviously, the slow response of the PEMFC [3], [4] needs to be compensated with a supercapacitor or a battery. A supercapacitor storage device is preferable due to its high power density, high dynamics, and long lifetime [5].

Many researchers have focused their studies on such systems. Riffonneau et al. [6] have studied the energy management of a grid connected PV/battery hybrid power plant. Jiang et al. [7] studied control based on an adaptive control with state machine estimation of an FC/Li-Ion battery hybrid power source, and Uzunoglu and Alam [8] have studied control based on a wavelet-based load sharing algorithm of an FC/SC hybrid power source.

A classical boost converter is often used as an FC converter and a PV converter [9], and a classical two-quadrant (bidirectional) converter is often used as a supercapacitor or battery converter. However, the classical converters will be limited when the power increases or at higher step-up ratios. As such, the use of parallel power converters (multiphase converters in parallel) with interleaving may offer better performance [10]. The interleaved converter can benefit both high current and high power density designs. It is ideal for merchant power applications because the reduced input ripple current and reduced output capacitor ripple current lessen the electrical stress on the dc capacitors.

Current work on controlling an FC/SC hybrid power plant is reported in [11], where a linear control using PI compensator was proposed for dc-link stabilization. Design controller parameters based on linear methods require a linear approximation [12], [13], where this is dependent on the operating point. Because the switching model of the hybrid power plant is nonlinear, it is natural to apply model-based nonlinear control strategies that directly compensate for system nonlinearity without requiring a linear approximation.

In the early 1990s, the flatness control theory was introduced by Fliess et al. [14] in a differential algebraic framework. It is simple, clear-cut, and appropriate for robustness, predictive control, trajectory planning, and constraints handling. Recently, this idea has been used in a variety of power electronic systems [15], [16]. Thounthong [16] has proved with real test bench results that the flatness-based control of a PV/supercapacitor power plant is absolutely robust.

The fast response, efficiency, and stability of the operation of hybrid power plants are of particular interest. In this work, a hybrid power generation system is studied, consisting of the following main components: a PV, proton exchange membrane FCs (PEMFC), and an SC as a high-power density device. In this study, a novel framework is proposed for the intelligent fuzzy logic-based flatness control approach of a solar-hydrogen power generation system with a supercapacitor storage device. The rest of the paper is structured as follows: Section II describes the hybrid energy system and modeling of the power plant that is studied in this work. Section III presents the proposed energy management algorithm, the proof of the flat system of the renewable energy power plant, and the control laws and system stability. Section IV presents test bench results for the proposed system. Finally, the paper ends with concluding remarks in Section V.

## II. SOLAR/HYDROGEN POWER PLANT

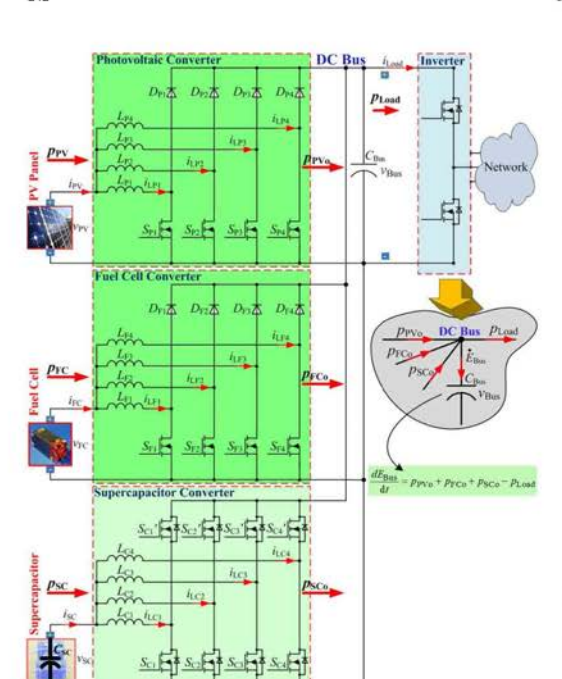
## A. Structure of Power Converters Studied

The power converter structure of the system studied in this paper is shown in Fig. 1. The FC and PV converters have four-phase parallel boost converters and the SC converter has four-phase parallel bidirectional converters (two-quadrant converters). For optimization in power converters, these converters connected in parallel, with an *interleaved switching technique*, increase the power processing capability and availability of the power electronic system [10].

For safety and high dynamics, the PV, FC, and SC converters are primarily controlled by inner current regulation loops classically. To ensure system stability, the dynamics of the inner regulation loops are also supposed to be much faster than those of the outer control loops [13]. These current control loops are supplied by three reference signals: iscrept, ipvrept, and ifcrept, generated by the control laws, presented hereafter.

## B. Mathematical Model of the Power Plant

We consider that the PV, FC, and SC currents follow their reference values perfectly. This is a classical assumption used in the cascade control structure in order to estimate the external control loop. However, the assumption error will be compensated by the intelligent external control loop. Then, the inner control loops of the PV, FC, and SC powers can be approximated as a unity gain. The PV power reference pyvref, the FC



Proposed circuit diagram of power plant supplied by an FC, a PV,

power reference  $p_{\text{FCREF}}$ , and the SC power reference  $p_{\text{SCREF}}$ 

$$p_{\text{PVREF}} = p_{\text{PV}} = v_{\text{PV}} \cdot i_{\text{PV}}$$
 (1)

$$p_{\text{FCREF}} = p_{\text{FC}} = v_{\text{FC}} \cdot i_{\text{FC}}$$
 (2)

$$p_{\text{SCREF}} = p_{\text{SC}} = v_{\text{SC}} \cdot i_{\text{SC}}.$$
 (3)

The PV panel, the FC generator, and the SC storage device function as controlled power sources. We assume here that there are only static losses in these converters, in which  $r_{PV}$ ,  $r_{FC}$ , and rsc represent the only static losses in the PV, the FC, and the SC converters, respectively. In real environment, the losses in converters are varied depending on many factors: temperature, current flow, etc. However, the estimation error will be compensated by the intelligent controller, presented hereafter. So, the dc-bus capacitive energy  $E_{\mathrm{Bus}}$  and the supercapacitive energy  $E_{\rm SC}$  can be written as

$$E_{\text{Bus}} = \frac{1}{2} C_{\text{Bus}} v_{\text{Bus}}^2, \quad E_{\text{SC}} = \frac{1}{2} C_{\text{SC}} v_{\text{SC}}^2.$$
 (4)

The total electrostatic energy  $E_T$  stored in the dc-bus capacitor  $C_{\mathrm{Bus}}$  and in the supercapacitor  $C_{\mathrm{SC}}$  can also be written as

$$E_T = \frac{1}{2}C_{\text{Bus}}v_{\text{Bus}}^2 + \frac{1}{2}C_{\text{SC}}v_{\text{SC}}^2.$$
 (5)

IEEE TRANSACTIONS ON SUSTAINABLE ENERGY, VOL. 4, NO. 1, JANUARY 2013

As portrayed in Fig. 1, the derivative of dc-bus capacitive energy  $E_{
m Bus}$  is given versus  $p_{
m PVo}, p_{
m FCo}, p_{
m SCo},$  and  $p_{
m Load}$  by the following differential equation:

$$\dot{E}_{\text{Bus}} = p_{\text{PVo}} + p_{\text{FCo}} + p_{\text{SCo}} - p_{\text{Load}}$$
 (6)

where

$$p_{\text{PVo}} = p_{\text{PV}} - r_{\text{PV}} \left(\frac{p_{\text{PV}}}{v_{\text{PV}}}\right)^2 \tag{7}$$

$$p_{FCo} = p_{FC} - r_{FC} \left( \frac{p_{FC}}{v_{FC}} \right)^2$$
(8)

$$p_{SCo} = p_{SC} - r_{SC} \left(\frac{p_{SC}}{v_{SC}}\right)^2 \tag{9}$$

$$p_{\text{Load}} = v_{\text{Bus}} \cdot i_{\text{Load}} = \sqrt{\frac{2E_{\text{Bus}}}{C_{\text{Rus}}}} \cdot i_{\text{Load}}$$
 (10)

$$p_{\text{FCo}} = p_{\text{FC}} - r_{\text{FC}} \left( \frac{p_{\text{FC}}}{v_{\text{FC}}} \right)^{2}$$

$$p_{\text{SCo}} = p_{\text{SC}} - r_{\text{SC}} \left( \frac{p_{\text{SC}}}{v_{\text{FC}}} \right)^{2}$$

$$p_{\text{Load}} = v_{\text{Bus}} \cdot i_{\text{Load}} = \sqrt{\frac{2E_{\text{Bus}}}{C_{\text{Bus}}}} \cdot i_{\text{Load}}$$

$$p_{\text{SC}} = v_{\text{SC}} \cdot i_{\text{SC}} = \sqrt{\frac{2E_{\text{SC}}}{C_{\text{SC}}}} \cdot i_{\text{SC}}.$$
(11)

## III. NONLINEAR MODEL-BASED CONTROL OF A POWER PLANT

## A. Energy Balance

The main control objectives are stability, high overall efficiency, and fast response. As for supplying energy to the load demanded and the charging storage device, the multivariable control here involves set-point control of the dc-bus voltage  $v_{\rm Bus}$ (representing the de-bus energy  $E_{
m Bus}$ , called "DC link stabilization") [11] and set-point control of the SC voltage vsc (representing the supercapacitive energy  $E_{SC}$ ).

The principle behind the proposed hybrid energy management lies in using the SCs (the fastest energy source) to supply the energy required to achieve the dc grid voltage regulation (or the dc bus energy regulation) [11]. Then, the PV and FC, although clearly the main energy source of the system, function as the generator that supplies energy for both the dc bus capacitor  $C_{\mathbf{Bus}}$  and the  $C_{\mathbf{SC}}$  to keep them charged.

## B. Flatness of the Power Plant Model

For the substantiation of flatness [17], [18], the system explanation from Section II is examined. To regulate the dc-bus voltage  $v_{\mathrm{Bus}}$  (DC link stabilization) and the SC voltage  $v_{SC}$ (state-of-charge), based on the flatness control theory introduced above, the flat outputs y, the control input variables u, and the state variables z are defined as

$$\mathbf{y} = \begin{bmatrix} y_1 \\ y_2 \end{bmatrix} = \begin{bmatrix} E_{\mathrm{Bus}} \\ E_T \end{bmatrix}, \quad \mathbf{u} = \begin{bmatrix} u_1 \\ u_2 \end{bmatrix} = \begin{bmatrix} p_{\mathrm{SCREF}} \\ p_{\mathrm{TREF}} \end{bmatrix}$$

$$\mathbf{x} = \begin{bmatrix} x_1 \\ x_2 \end{bmatrix} = \begin{bmatrix} v_{\mathrm{Bus}} \\ v_{\mathrm{SC}} \end{bmatrix}$$
(12)

where  $p_{TREF}$  is the total power from the FC and PV array. From (4) and (5), the state variables z can be written as

$$x = \begin{bmatrix} x_1 \\ x_2 \end{bmatrix} = \begin{bmatrix} \sqrt{\frac{2y_1}{C_{\text{Bus}}}} \\ \sqrt{\frac{2(y_2 - y_1)}{C_{\text{SC}}}} \end{bmatrix} = \begin{bmatrix} \varphi_1(y_1) \\ \varphi_2(y_1, y_2) \end{bmatrix}. \tag{13}$$

THOUNTHONG et al.: INTELLIGENT MODEL-BASED CONTROL OF A STANDALONE PV/FC POWER PLANT WITH SC ENERGY STORAGE

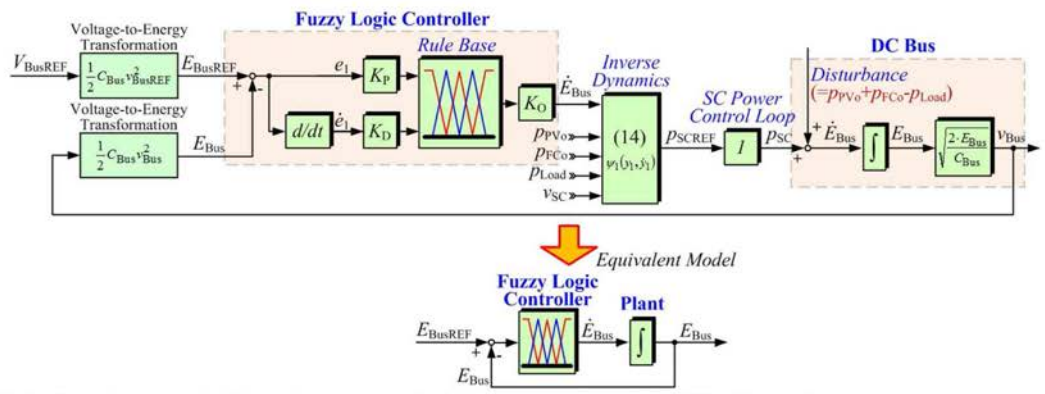


Fig. 2. Control law based on the differential flatness theory of the dc-bus energy regulation for PV/FC/SC hybrid power plant.

From (6) to (11), the control input variables  $\boldsymbol{u}$  can be calculated from the flat output  $\boldsymbol{y}$  and its time derivatives

$$u_{1} = 2p_{\text{SCLim}}$$

$$\cdot \left[ 1 - \sqrt{1 - \left( \frac{\dot{y}_{1} + \sqrt{\frac{2y_{1}}{C_{\text{Bus}}}} \cdot i_{\text{Load}} - p_{\text{FCo}} - p_{\text{PVo}}}{p_{\text{SCLim}}} \right)} \right]$$

$$= \psi_{1}(y_{1}, \dot{y}_{1}) \qquad (14)$$

$$u_{2} = 2p_{\text{TMax}} \cdot \left[ 1 - \sqrt{1 - \left( \frac{\dot{y}_{2} + \sqrt{\frac{2y_{1}}{C_{\text{Bus}}}} \cdot i_{\text{Load}}}{p_{\text{TMax}}} \right)} \right]$$

$$= \psi_{2}(y_{1}, \dot{y}_{2}) \qquad (15)$$

where

$$p_{\text{SCLim}} = \frac{v_{\text{SC}}^2}{4r_{\text{SC}}}, \quad p_{\text{TMax}} = \frac{v_T^2}{4r_T}.$$
 (16)

 $p_{\rm SCLim}$  is the limited maximum power from the SC converter,  $v_T$  is the virtual voltage from the FC and PV power generators, and  $r_T$  is the virtual static losses in the FC and PV power converters.

In fact.

$$p_{\text{TMax}} = p_{\text{FCMax}} + p_{\text{PVMax}} \tag{17}$$

where  $p_{FCMax}$  is the maximum FC power and  $p_{PVMax}$  is the maximum PV power.

Thus, it is understandable that  $x_1 = \varphi_1(y_1), x_2 = \varphi_2(y_1, y_2), u_1 = \psi_1(y_1, \dot{y}_1)$ , and  $u_2 = \psi_2(y_1, \dot{y}_2)$ . The proposed reduced order model can be studied as a flat system [17], [18].

## C. DC Link Stabilization

Fuzzy control algorithms offer many advantages over traditional controls because they give fast convergence, are parameter insensitive, and accept noisy and inaccurate signals [19], [20]. In recent years, it has been used in many control applications where the system is complex [21], [22]. The control objective is to regulate the dc bus voltage  $v_{\rm Bus}$  or the dc bus energy  $E_{\rm Bus}(=y_1)$ . The controller contains a Takagi–Sugeno (T-S) inference engine and two fuzzy inputs: the energy error  $e_1(=y_{\rm IREF}-y_1)$  and the differential energy error  $\dot{e}_1$ , which are carefully adjusted using the proportional gain  $K_P$  and the derivative gain  $K_D$ , respectively. In addition, the fuzzy output level can be set by the proportional gain  $K_O$  (Fig. 2).

Triangular and trapezoidal membership functions are chosen for both of the fuzzy inputs, as shown in Fig. 3(a). There are seven membership functions for each input, including NB (Negative Big), NM (Negative Medium), NS (Negative Small), Z (Zero), PB (Positive Big), PM (Positive Medium), and PS (Positive Small). For the singleton output membership function, the zero-order Sugeno model is used, where the membership functions are specified symmetrically, as follows: NB = -1, NM = -0.66, NS = -0.33, Z = 0, PB = 1, PM = 0.66, and PS = 0.33, as presented in Fig. 3(b).

For the rule base, expert suggestions, an experimental approach, and a trial and error technique were used to define the relationships between the inputs and the output. The data representation was in the form of an *IF-THEN* rule, as shown in the following example:

IF 
$$e_{1i}$$
 is NS and  $\dot{e}_{1i}$  is NS THEN  $\mathbf{z_i}(=\mathtt{output})$  is NB.

As shown in Fig. 3(c), the total number of rule bases is, therefore, equal to 49 rules. To obtain the output of the controller, the center of gravity method for the *COGS* of the singletons is utilized as

$$U = \frac{\sum_{i=1}^{N} w_i z_i}{\sum_{i=1}^{N} w_i}$$
 (18)

where the weights  $(w_i)$  can be retrieved from

$$w_i = \max(e_{1i}, \dot{e}_{1i}). \tag{19}$$

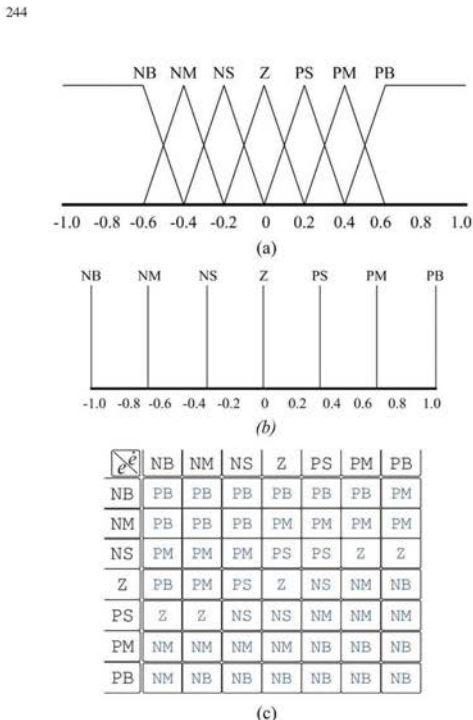


Fig. 3. Rule base and membership functions. (a) Input membership functions. (b) Output membership function. (c) Rule base.

## D. Charging Supercapacitor

Because the SC energy storage has a massive size capacity, and the supercapacitive energy is defined as a slower dynamic variable than the dc-bus energy variable. Then, the proposed control law is [23], [24]

$$(\dot{y}_2 - \dot{y}_{2REF}) + K_{21}(y_2 - y_{2REF}) = 0.$$
 (20)

This yields

$$\dot{y}_2 = \dot{y}_{2REF} + K_{21}(y_{2REF} - y_2)$$
 (21)

where  $y_{2REF}$  is the reference of total electrostatic energy, refer to (5), and  $K_{21}$  is the control parameter.

From (20), if we define  $e_2 = y_2 - y_{2REF}$ ,  $K_{21} = 1/\tau_S$ , we obtain

$$\tau_S \cdot \dot{e}_2 + e_2 = 0. \tag{22}$$

Substituting the expression for  $\dot{y}_2$  from (21) into (15) gives the equation for the closed-loop static state feedback, in which one obtains the inverse dynamics

$$u_2 = \psi_2(y_1, \dot{y}_2) = p_{\text{TREF}}$$
  
=  $p_{\text{PVDEM}} + p_{\text{FCDEM}}$  (23)

where  $p_{\text{PVDEM}}$  is the PV power demand and  $p_{\text{FCDEM}}$  is the FC power demand.

The total energy control law (or the SC energy control law) generates a total power reference **p**<sub>TREF</sub>, as shown in Fig. 4.

IEEE TRANSACTIONS ON SUSTAINABLE ENERGY, VOL. 4, NO. 1, JANUARY 2013

First,  $p_{TREF}$  is considered as the PV power demand  $p_{PVDEM}$ . It must be limited in level, within an interval maximum  $p_{PVMax}$  (maximum power point tracking MPPT) and minimum  $p_{PVMin}$  (set to 0 W). Several approaches have been devised for tracking MPP accurately for PV cells [25], [26]. Some of the popular ones are the perturbation and observation algorithm (P&O) method [27]. Based on P&O MPPT, the pseudocode for the PV power saturation function studied here is described in ALGORITHM I, where  $\Delta I_{PV}$  is the defined PV current step size and  $\Delta t_{PV}$  is the sampling time. Note that this sampling time must be higher than a main program sampling time.

## ALGORITHM I: MPPT for PV

```
BEGIN
     READ p_{PVDEM}(t)
     READ v_{PV}(t)
     READ i_{PV}(t)
    p_{\mathrm{PV}}(t) = v_{\mathrm{PV}}(t) \times i_{\mathrm{PV}}(t)
    p_{\text{PV}}(t - \Delta t_{\text{PV}}) = v_{\text{PV}}(t - \Delta t_{\text{PV}}) \times i_{\text{PV}}(t - \Delta t_{\text{PV}})
     IF p_{\text{PV}}(t) \geq p_{\text{PV}}(t - \Delta t_{\text{PV}}) THEN
          IF i_{\text{PV}}(t) \geq i_{\text{PV}}(t - \Delta t_{\text{PV}}) THEN
                i_{\mathrm{PVMax}}(t) = i_{\mathrm{PV}}(t) + \Delta I_{\mathrm{PV}}
          ELSE
                i_{\mathrm{PVMax}}(t) = i_{\mathrm{PV}}(t) - \Delta I_{\mathrm{PV}}
          ELSEIF
     ELSE
          IF i_{\rm PV}(t) \geq i_{\rm PV}(t - \Delta t_{\rm PV}) THEN
                i_{\mathrm{PVMax}}(t) = i_{\mathrm{PV}}(t) - \Delta I_{\mathrm{PV}}
                i_{\mathrm{PVMax}}(t) = i_{\mathrm{PV}}(t) + \Delta I_{\mathrm{PV}}
          ELSEIF
     ENDIE
    p_{\mathrm{PVMax}}(t) = v_{\mathrm{PV}}(t) \times i_{\mathrm{PVMax}}(t)
    p_{\text{PVREF}}(t) = \min[p_{\text{PVDEM}}(t), p_{\text{PVMax}}(t)]
    v_{\rm PV}(t - \Delta t_{\rm PV}) = v_{\rm PV}(t)
    i_{\mathrm{PV}}(t - \Delta t_{\mathrm{PV}}) = i_{\mathrm{PV}}(t)
```

Second, the difference between the total power reference  $p_{TREF}$  and the PV power reference  $p_{PVREF}$  is the FC power demand  $p_{FCDEM}$ . It must be limited in level, within an interval maximum  $p_{FCMax}$  and minimum  $p_{FCMin}$  (set to 0 W) and limited in dynamics to respect the constraints that are associated

THOUNTHONG et al.: INTELLIGENT MODEL-BASED CONTROL OF A STANDALONE PV/FC POWER PLANT WITH SC ENERGY STORAGE

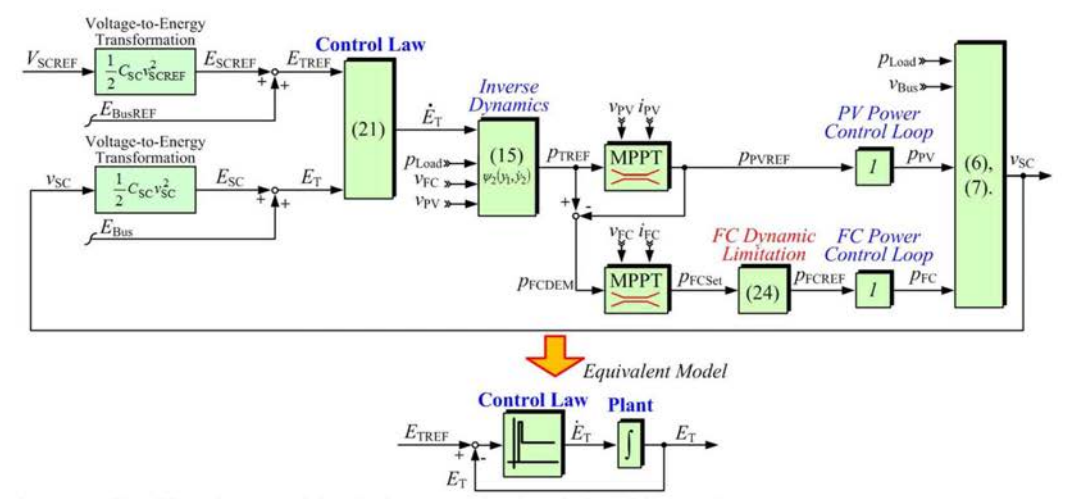


Fig. 4. Control law of the total energy regulation (charging supercapacitor) for PV/FC/SC hybrid power plant.

with the FC [4]. Based on P&O MPPT, the pseudocode for the FC power saturation function is similar to ALGORITHM I.

The typical polarization curve of a PEMFC is dependent on many factors: temperature, humidity, cell current, etc., [28], [29]. Moreover, the lifetime target requires PEMFCs to achieve 5000 h for mobile and 40 000 h for stationary applications. Normal degradation targets require less than 10% loss in the efficiency of the fuel cell system at the end of life, and a degradation rate of  $2-10~\mu\text{V}\cdot\text{h}^{-1}$  [30], [31]. For these reasons, the MPPT for FC is obligatory. So, to limit the transient FC power [32], [33], a low-pass filter (second order) is employed such that the power demand  $p_{\text{FCSet}}$  from MPPT is always limited by

$$p_{\text{FCREF}}(t) = p_{\text{FCSet}}(t) \cdot \left(1 - e^{-\frac{t}{\tau_1}} - \frac{t}{\tau_1} e^{-\frac{t}{\tau_1}}\right) \tag{24}$$

where  $\tau_1$  is the control parameter.

## IV. PERFORMANCE VALIDATIONS

## A. Test Bench Description

To authenticate the performance of the modeling and control system, a test bench was implemented. The small-scale test bench of the renewable power plant was implemented in our laboratory, as presented in Fig. 5. The prototype FC converter of 1 kW, the PV converter of 0.8 kW, and the SC converter of 2 kW (refer to Fig. 1) were realized in the laboratory. Specifications of the real power sources and storage device are detailed in Table I. Note that the PV panel is installed on the roof of the laboratory building (Fig. 5). It means that the PV energy production is directly from the sun.

The efficiency of each converter is around 85%, because the implemented converters are hard-switching converters. So, the power losses can be observed in the following experimental results. To improve the converter efficiency, soft-switching converters may be effective solutions for future work.

### B. Control Description

The parameters associated with the de-bus energy regulation loop are summarized in Table II. Note that  $K_O$  fuzzy logic controller is negative value because of the membership function and rule base as presented in Fig. 3. Parameters associated with the SC energy regulation loop are detailed in Table III. The FC, PV, and SC current regulation loops were realized by analog circuits. The two energy control loops, which generate current references  $i_{FCREF}, i_{PVREF}$  and  $i_{SCREF}$ , were implemented in the real time card dSPACE DS1104 (see Fig. 5), through the mathematical environment of Matlab-Simulink, with a sampling frequency of 25 kHz.

## C. Experimental Results

Fig. 6 presents waveforms that are obtained during the long load cycles measured on March 29, 2011. The experimental tests were carried out by connecting a dc link loaded by an electronic load. The load will be varied in order to emulate the real environment: light load, over load, positive transition ( $\uparrow$ ), and negative transition ( $\downarrow$ ). The data show the dc bus voltage, the FC voltage, the load power, the SC power, the FC power, the PV power, the SC current, the FC current, the PV current, and the SC voltage. In the initial state, the small load power is equal to 280 W, and the SC storage device is full of charge, i.e.,  $v_{\text{SC}} = V_{\text{SCNom}} = V_{\text{SCREF}} = 25 \text{ V}$ ; as a result, the photovoltaic source supplies power for the load of 280 W (because  $p_{\text{PVMax}} > p_{\text{PVDEM}}$ , then  $p_{\text{PVREF}} = p_{\text{PVDEM}}$ ), and the FC and SC powers are zero.

At 9:00:50, the large load power steps from 280 W to the final constant power of 900 W (positive load power transition). The following observations are made:

- 1) The SC supplies most of the transient step load.
- Concurrently, the photovoltaic power increases to a maximum power point (MPP) of around 350 W, which is limited by the maximum power point tracker (MPPT), because ppvMax < ppvDEM, then ppvREF = ppvMax.</li>

IEEE TRANSACTIONS ON SUSTAINABLE ENERGY, VOL. 4, NO. 1, JANUARY 2013

TABLE I

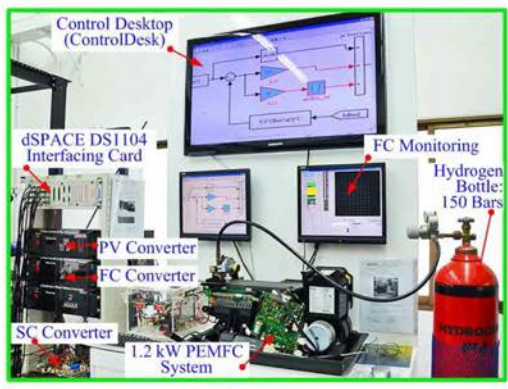






Fig. 5. Photograph of the experimental setup.

- At the same time, the FC power increases with limited dynamics to MPP of around 430 W.
- 4) The input from the SC, which supplies most of the transient power that is required during the stepped load, slowly decreases and the unit remains in a discharge state after the load step because the steady-state load power (approximately 900 W) is greater than the total power supplied by the photovoltaic array and fuel cell. This state is known as the ride-through mode.

After that, at 9:02:10, the load power steps from 900 to 280 W (negative transition) and  $V_{\rm SCREF} (= 25 \text{ V}) > v_{\rm SC} (= 17 \text{ V})$ . As a result, the SC changes its state from discharging to charging, demonstrating the four phases.

SPECIFICATIONS OF POWER SOURCES AND STORAGE DEVICE Fuel Cell System (by Ballard Power Systems Inc): Rated Power 1,200 Rated Current A V Rated Voltage 26 Photovoltaic Array (by Ekarat Solar Company): Number of Panels in Parallel Panel Open Circuit Voltage 33.5 Panel Rated Voltage 26 Panel Rated Current w Panel Rated Power 200 Array Rated Power 800

# Supercapacitor Bank (by Maxwell Technologies Comp): (Cell Model: BCAP1200) Number of Cells in Series 12

 Number of Cells in Series
 12

 Cell Capacity
 1,200
 F

 Cell Maximum Voltage
 2.7
 V

 Bank Capacity ( $C_{SC}$ )
 100
 F

 Bank Maximum Voltage
 32
 V

IADLE II		
DC-Bus Energy	CONTROL	LOOP PARAMETERS

TABLEII

$V_{\mathrm{BusREF}}$	60	V
$C_{\mathrm{Bus}}$	12200	μF
Kp	0.15	
$K_{\rm D}$	0.15	
Ko	-200	
rpv.	0.13	Ω
r <sub>FC</sub>	0.13	Ω
rsc	0.08	Ω
$V_{\text{SCMax}}$	32	V
$V_{\text{SCMin}}$	15	V
I <sub>SCRated</sub>	150	A

TABLE III
SUPERCAPACITIVE ENERGY CONTROL LOOP PARAMETERS

$V_{\text{SCREF}}$	25	V
$C_{SC}$	100	F
$K_{21}$	0.1	W·J·1
PFCMin	0	W
I <sub>FCMax</sub> (Rated)	46	A
$I_{\text{FCMin}}$	0	A
$\tau_1$	5	S

- First, the FC and PV still supply their total limited maximum powers for driving the load and for charging the SC, intelligently.
- Second, at 9:02:35 (v<sub>SC</sub> = 23.5 V), the SC is nearly charged at 25 V; which then reduces the charging power. As a result, the FC power is reduced to zero.
- Third, at 9:03:00 (v<sub>SC</sub> = 24.5 V), the SC is nearly fully charged at 25 V; as a result, the PV power is reduced.
- 4) Fourth, at 9:03:20, the SC is fully charged (V<sub>SCREF</sub> = v<sub>SC</sub> = 25.0 V). As a result, the FC and SC powers are zero; the PV source supplies power for the load of 280 W.

During the experiment, the FC maximum power is limited by the MPPT and the PV maximum power is limited by the MPPT. Exceptionally, one can observe that the power plant is always energy balanced ( $p_{\text{Load}} = p_{\text{PV}} + p_{\text{FC}} + p_{\text{SC}}$ ) by the proposed original control algorithm.

The oscilloscope waveforms in Fig. 7 show the dynamic response of the de bus voltage dynamics to the large load power

THOUNTHONG et al.: INTELLIGENT MODEL-BASED CONTROL OF A STANDALONE PV/FC POWER PLANT WITH SC ENERGY STORAGE

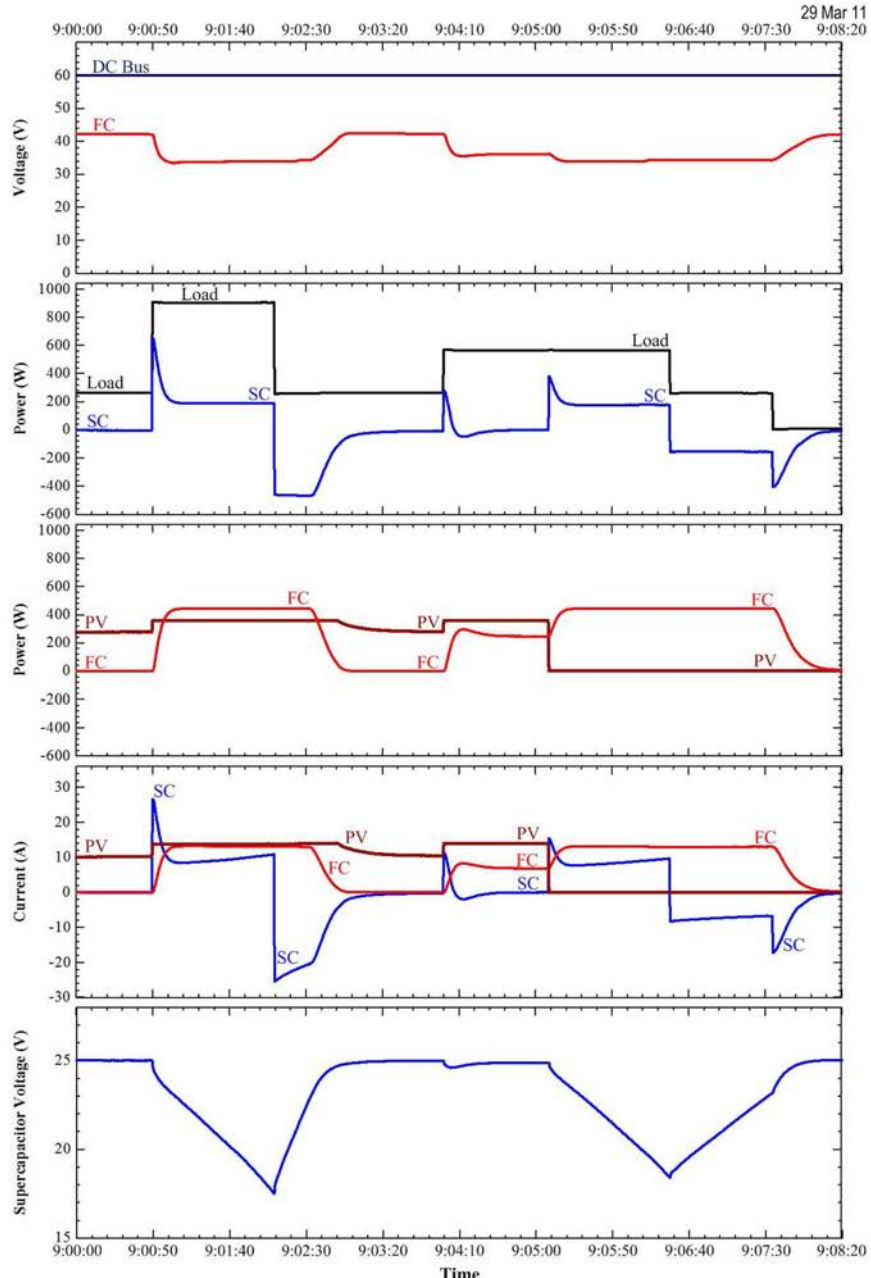
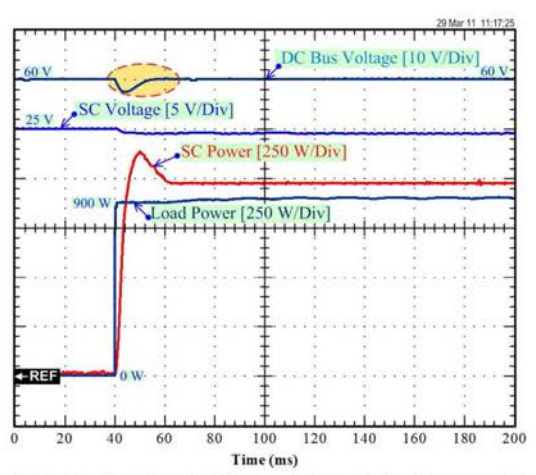


Fig. 6. Experimental results: Power plant response during load cycles.

demands (disturbance) from 0 to 900 W. The oscilloscope screens show the de bus voltage, the SC voltage, the load power, and the SC power. The PV and FC power dynamics were purposely limited, forcing the SC to supply the transient

load power demand. The proposed fuzzy-logic controller shows good stability and an optimum response (no oscillation and short settling time) for the regulation of the dc bus voltage to the desired reference of  $60~\rm V$ .

IEEE TRANSACTIONS ON SUSTAINABLE ENERGY, VOL. 4, NO. 1, JANUARY 2013



248

Fig. 7. Experimental results of the dynamic characteristics of the power plant during a step load from 0 to 900 W

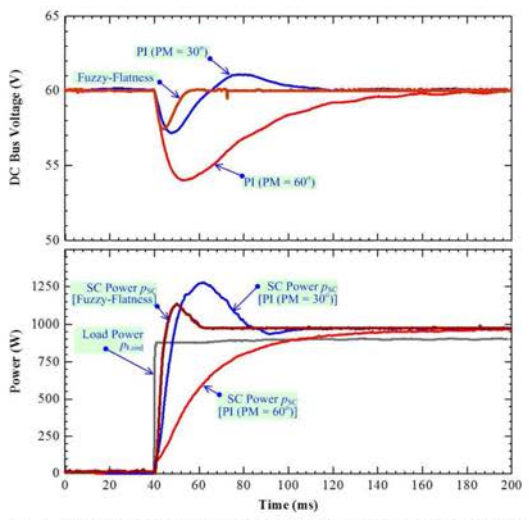


Fig. 8. Comparison of the fuzzy-flatness based control law with a linear PI control law during a large load step

Finally, to compare the performance of the proposed control law, a traditional linear PI control method presented in [11] was also implemented on the test bench. In order to give a rational comparison between the methods, the parameters of the linear controller  $K_P$  and  $K_I$  were tuned to obtain the best possible performance. The desired phase margin (PM) was tuned at 30° and 60°. This result was compared to the fuzzy-flatness-based control. Fig. 8 shows experimental results obtained for both controllers during the large load step. The fuzzy-flatness-based control shows good stability and optimum response of the dc-bus voltage regulation to its desired reference of 60 V. Although dynamic response of the linear control law could be improved relative to that shown in the figures, this enhancement comes at the expense of a reduced stability margin (overshoot and oscillation). From these results, we conclude that fuzzy-flatness-based control provides better performance than the classical PI controller.

## V. CONCLUSION

The key contribution of this paper is to authenticate the intelligent fuzzy logic control based on differential flatness estimation of a PV/FC/SC hybrid power plant for standalone applications. The prototype power plant studied was composed of a PEMFC system (1200 W), a PV array (800 W), and an SC module (100 F). Its working principle, analysis, and design procedure were presented. The PV is the main source, while the FC serves as a support source to compensate for the uncertainties of the PV source in the steady state. The SC functions as a storage device (or an auxiliary source) to compensate for the uncertainties of the PV and FC sources in the steady state and transient

Using the intelligent fuzzy logic control for dc link stabilization based on the flatness property, we proposed simple solution to the fast response and stabilization problems in the nonlinear power electronic system. This strategy is based on a standard de link voltage regulation, which is simpler than standard state machines used for hybrid source control, and free of chattering problems. This is the novel concept for this kind of application. Experimental results authenticated the control algorithm and control laws.

#### ACKNOWLEDGMENT

The authors would like to thank Dr. P. Sethakul (KMUTNB) and Dr. S. Pierfederici (Université de Lorraine) for their valuable comments and suggestions about power electronics and

## REFERENCES

- [1] M. H. Nehrir, C. Wang, K. Strunz, H. Aki, R. Ramakumar, J. Bing, Z. Miao, and Z. Salameh, "A review of hybrid renewable/alternative energy systems for electric power generation: Configurations, control, and applications," *IEEE Trans. Sustain. Energy*, vol. 2, no. 4, pp. 392-403, Oct. 2011
- [2] P. Thounthong, V. Chunkag, P. Sethakul, S. Sikkabut, S. Pierfederici, and B. Davat, "Energy management of fuel cell/solar cell/supercapacitor hybrid power source," *J. Power Sources*, vol. 196, no. 1, pp. 313-324, Jan. 2011.
- [3] A. Ravey, N. Watrin, B. Blunier, D. Bouquain, and A. Miraoui, "Energy-source-sizing methodology for hybrid fuel cell vehicles based on statistical description of driving cycles," *IEEE Trans. Veh. Technol.*, vol. 60, no. 9, pp. 4164–4174, Nov. 2011.

  [4] T. Azib, O. Bethoux, G. Remy, and C. Marchand, "Saturation management of a controlled fuel-cell/ultracapacitor hybrid vehicle," *IEEE*
- Trans. Veh. Technol., vol. 60, no. 9, pp. 4127–4138, Nov. 2011.

  [5] A. S. Weddell, G. V. Merrett, T. J. Kazmierski, and B. M. Al-Hashimi, "Accurate supercapacitor modeling for energy harvesting wireless sensor nodes," IEEE Trans. Circuits Syst. II, Exp. Brief, vol. 58, no. 12, pp. 911–915, Dec. 2011.
- [6] Y. Riffonneau, S. Bacha, F. Barruel, and S. Ploix, "Optimal power flow management for grid connected PV systems with batteries," *IEEE*
- Trans. Sustain. Energy, vol. 2, no. 3, pp. 309–420, Jul. 2011.
   Z. Jiang, L. Gao, and R. A. Dougal, "Adaptive control strategy for active power sharing in hybrid fuel cell/battery power sources," *IEEE Trans. Energy Convers*, vol. 22, no. 2, pp. 507–515, Jun. 2007.
   M. Uzunoglu and M. S. Alam, "Modeling and analysis of an FC/UC hy-
- brid vehicular power system using a novel-wavelet-based load sharing algorithm," *IEEE Trans. Energy Convers.*, vol. 23, no. 1, pp. 263–272, Mar. 2008

- [9] W. Na, T. Park, T. Kim, and S. Kwak, "Light fuel-cell hybrid electric vehicles based on predictive controllers," *IEEE Trans. Veh. Technol.*, vol. 60, no. 1, pp. 89–97, Jan. 2011.
  [10] P. Thounthong and S. Pierfederici, "A new control law based on the differential flatness principle for multiphase interleaved DC-DC con-
- verter," IEEE Trans. Circuits Syst. II, Exp. Briefs, vol. 57, no. 11, pp. 903-907, Nov. 2010.
- [11] P. Thounthong, S. Raël, and B. Davat, "Control strategy of fuel cell and supercapacitors association for distributed generation system," *IEEE Trans. Ind. Electron.*, vol. 54, no. 6, pp. 3225–3233, Dec. 2007.

  [12] C. Xia, X. Gu, T. Shi, and Y. Yan, "Neutral-point potential balancing of the control of t
- three-level inverters in direct-driven wind energy conversion system,
- IEEE Trans. Energy Convers., vol. 26, no. 1, pp. 18–29, Mar. 2011.
  [13] H. Zhou, G. Yang, and J. Wang, "Modeling, analysis, and control for the rectifier of hybrid HVdc systems for DFIG-based wind farms," IEEE Trans. Energy Convers., vol. 26, no. 1, pp. 340–353, Mar. 2011.
  [14] M. Fliess, J. Levine, Ph. Martin, and P. Rouchon, "A Lie-Bäcklund ap-
- proach to equivalence and flatness of nonlinear systems," *IEEE Trans. Automat. Contr.*, vol. 44, no. 5, pp. 922–937, May 1999.

  [15] M. Zandi, A. Payman, J.-Ph. Martin, S. Pierfederici, B. Davat, and
- F. Meibody-Tabar, "Energy management of a fuel cell/supercapacitor/ battery power source for electric vehicular applications," *IEEE Trans.*
- battery power source for electric vehicular applications," *IEEE Trans. Veh. Technol.*, vol. 60, no. 2, pp. 433–443, Feb. 2011.
  [16] P. Thounthong, "Model based-energy control of a solar power plant with a supercapacitor for grid-independent applications," *IEEE Trans. Energy Convers.*, vol. 26, no. 4, pp. 1210–1218, Dec. 2011.
  [17] A. Gensior, T. M. P. Nguyen, J. Rudolph, and H. Güldner, "Flatness-based loss optimization and control of a doubly fed induction generator system," *IEEE Trans. Control Syst. Technol.*, vol. 19, no. 6, pp. 1457–1466, Nov. 2011. 1457-1466, Nov. 2011. C. P. Tang, P. T. Miller, V. N. Krovi, J.-C. Ryu, and S. K. Agrawal,
- (18) C. P. Lang, P. T. Miller, V. N. Krovi, J.-C. Ryu, and S. K. Agrawal, "Differential-flatness-based planning and control of a wheeled mobile manipulator—Theory and experiment," *IEEE/ASME Trans. Mechatronics*, vol. 16, no. 4, pp. 768–773, Aug. 2011.
  [19] M. Datta, T. Senjyu, A. Yona, T. Funabashi, and C.-H. Kim, "A frequency-control approach by photovoltaic generator in a PV-diesel hybrid power system," *IEEE Trans. Energy Convers.*, vol. 26, no. 2, pp. 1018.
  [10] S. G. Li, S. M. Shaght, F. C. Walth, and C. N. Zhang, "Engrave and Conversion of the converse of the conver
- [20] S. G. Li, S. M. Sharkh, F. C. Walsh, and C. N. Zhang, "Energy and battery management of a plug-in series hybrid electric vehicle using fuzzy logic," *IEEE Trans. Veh. Technol.*, vol. 60, no. 8, pp. 3571–3585, Oct. 2011.
- [21] U.-C. Moon and K. Y. Lee, "An adaptive dynamic matrix control with fuzzy-interpolated step-response model for a drum-type boiler-turbine system," *IEEE Trans. Energy Convers.*, vol. 26, no. 2, pp. 393–401,
- Jun. 2011.[22] A. Elmitwally and M. Rashed, "Flexible operation strategy for an is [22] A. Elmitwally and M. Rashed, "Flexible operation strategy for an isolated PV-diesel microgrid without energy storage," *IEEE Trans. Energy Convers.*, vol. 26, no. 1, pp. 235–244, Mar. 2011.
  [23] A. Payman, S. Pierfederici, and F. Meibody-Taba, "Energy control of super-capacitor/fuel cell hybrid power source," *Energy Convers. Manage.*, vol. 49, no. 6, pp. 1637–1644, Jun. 2008.
  [24] P. Thounthong, S. Pierfederici, and B. Davat, "Analysis of differential flatness-based control for a fuel cell hybrid power source," *IEEE Trans. Energy Conwers*, vol. 25, no. 3, no. 909, 920, 820, 2012.

- flatness-based control for a fuel cell hybrid power source," *IEEE Trans. Energy Convers.*, vol. 25, no. 3, pp. 909–920, Sep. 2010.
  [25] G. Farivar and B. Asaei, "A new approach for solar module temperature estimation using the simple diode model," *IEEE Trans. Energy Convers.*, vol. 26, no. 4, pp. 1118–1126, Dec. 2011.
  [26] P. Lei, Y. Li, and J. E. Seem, "Sequential ESC-based global MPPT control for photovoltaic array with variable shading," *IEEE Trans. Sustain. Energy*, vol. 2, no. 3, pp. 348–358, Jul. 2011.
  [27] F.-S. Pai, R.-M. Chao, S. H. Ko, and T.-S. Lee, "Performance evaluation of parabolic prediction to maximum power point tracking for PV array," *IEEE Trans. Sustain. Energy*, vol. 2, no. 1, pp. 60–68, Jan. 2011.
- array," IEEE Trans. Sustain. Energy, vol. 2, no. 1, pp. 60-68, Jan. 2011. [28] F. Gao, B. Blunier, M. G. Simões, and A. Miraoui, "PEM fuel cell stack modeling for real-time emulation in hardware-in-the-loop appli-" IEEE Trans. Energy Convers., vol. 26, no. 1, pp. 184-194,
- [29] C. Kunusch, P. F. Puleston, M. A. Mayosky, and A. P. Husar, "Control-oriented modeling and experimental validation of a PEMFC generation system," IEEE Trans. Energy Convers., vol. 26, no. 3, pp. 851-861,
- [30] X.-Z. Yuan, H. Li, S. Zhang, J. Martin, and H. Wang, "A review of polymer electrolyte membrane fuel cell durability test protocols," *J. Power Sources*, vol. 196, no. 22, pp. 9107–9116, Nov. 2011.

- [31] X.-Z. Yuan, S. Zhang, J. C. Sun, and H. Wang, "A review of accelerated
- [31] X.-Z. Yuan, S. Zhang, J. C. Sun, and H. Wang, "A review of accelerated conditioning for a polymer electrolyte membrane fuel cell," *J. Power Sources*, vol. 196, no. 22, pp. 9097–9106, Nov. 2011.
  [32] J. S. Martinez, D. Hissel, M. C. Péra, and M. Amiet, "Practical control structure and energy management of a testhed hybrid electric vehicle," *IEEE Trans. Veh. Technol.*, vol. 60, no. 9, pp. 4139–4151, Nov. 2011.
  [33] N. Bizon, "A new topology of fuel cell hybrid power source for efficient operation and high reliability," *J. Power Sources*, vol. 196, no. 6, pp. 3260, 3270, Mar. 2011.
- 3260-3270, Mar. 2011.



Phatiphat Thounthong (M'09) received the B.S. and M.E. degrees in electrical engineering from King Mongkut's Institute of Technology North Bangkok (KMITNB), Bangkok, Thailand, in 1996 and 2001, respectively, and the Ph.D. degree in electrical engineering from Institut National Polytechnique de Lorraine (INPL)-Université de Lorraine, Nancy-Lorraine. France in 2005.

Currently, he is an Associate Professor in Department of Teacher Training in Electrical Engineering (TE), King Mongkut's University of Technology North Bangkok (KMUTNB). His current research interests include power

electronics, electric drives, and electrical devices (FC, PV, wind turbine, batteries, and SC).



Arkhom Luksanasakul received the B.S. degree in technical education (electrical engineering) from Rajamangala Institute of Technology Nonthaburi Campus, Thailand, in 2000, and received the M.S. degree in technical education (electrical technology) from King Mongkut's Institute of Technology North Bangkok, Thailand, in 2004.

He is currently working toward the Ph.D. degree

in electrical education in Department of Teacher Training in Electrical Engineering, King Mongkut's

University of Technology North Bangkok, Thailand. (PID, Fuzzy, Auto-tuning).



Poolsak Koseeyaporn received the B.S. degree in electrical engineering from King Mongkut's Institute of Technology North Bangkok, Thailand, in 1996, and the M.S. and Ph.D. degrees in electrical engi-neering from Vanderbilt University, Nashville, TN, in 1999 and 2003, respectively.

Currently, he is an Assistant Professor of Electrical Engineering, Department of Teacher Training in electrical engineering, Faculty of Technical Ed-ucation, King Mongkut's University of Technology North Bangkok (KMUTNB), Thailand. His research

interests are control and robotics, engineering, and science learning.



Bernard Davat (M'89) received the Engineer degree from Ecole Nationale Supérieure d'Elec-trotechnique, d'Electronique, d'Informatique, trotechnique, d'Electronique, d'Informatique d'Hydraulique et des Telecommunications (EN-SEEIHT), Toulouse, France, in 1975, and the Ph.D. and Docteur d'Etat degrees in elecrical engineering from Institut National Polytechnique de Toulouse (INPT), Toulouse, in 1978 and 1984, respectively.

From 1980 to 1988, he was a Researcher at French National Center for Scientific Research (CNRS),

Laboratoire d'Electrotechnique et d'Electronique Industrielle (LEEI). Since 1988, he has been a Professor at Institut National Polytechnique de Lorraine- Université de Lorraine, Nancy-Lorraine, France. His current research interests include power electronics, drives, and new electrical devices (fuel cell and supercapacitor). Electrical Power and Energy Systems 54 (2014) 454-464



Contents lists available at ScienceDirect

## Electrical Power and Energy Systems

journal homepage: www.elsevier.com/locate/ijepes



## Performance investigation of linear and nonlinear controls for a fuel cell/supercapacitor hybrid power plant



Phatiphat Thounthong a,\*, Pietro Tricoli b, Bernard Davat C

- <sup>a</sup>Renewable Energy Research Centre, Department of Teacher Training in Electrical Engineering, King Mongkut's University of Technology North Bangkok, 1518, Pracharat 1 Road, Wongsawang, Bangsue, Bangkok 10800, Thailand
- vvongsavvang, sangsue, sangsoe 10000, Indiatia "School of Electronic, Electrical and Computer Engineering, University of Birmingham, Gisbert Kapp Building, B15 2TT Birmingham, United Kingdom "Groupe de Recherche en Electrotechnique et Electronique de Nancy, Université de Lorraine, 2, Avenue de la Forêt de Haye, Vandœuvre-lés-Nancy, Lorraine 54516, France

#### ARTICLE INFO

Article history. Received 20 August 2012 Received in revised form 24 July 2013 Accepted 25 July 2013

Keywords: Converters Fuel cells Nonlinear control Supercapacitor Voltage control

#### ABSTRACT

In this paper, linear proportional-integral (PI) and nonlinear flatness-based controllers for dc link stabilization for fuel cell/supercapacitor hybrid power plants are compared. For high power applications, 4-phase parallel boost converters are implemented with a switching interleaving technique for a fuel cell (FC) converter, and 4-phase parallel bidirectional converters are implemented with a switching interleaving technique for a supercapacitor converter in the laboratory. As controls, mathematical models (reduced-order models) of the FC converter and the supercapacitor converter are given. The prototype small-scale power plant studied is composed of a PEMFC system (the Nexa Ballard FC power generator: 1.2 kW, 46 A) and a supercapacitor module (100 F, 32 V, based on Maxwell Technologies Company). Simulation (by Matlab/Simulink) and experimental results demonstrate that the nonlinear differential flatness-based control provides improved dc bus stabilization relative to a classical linear PI control

© 2013 Elsevier Ltd. All rights reserved.

## 1. Introduction

FCs have experienced remarkably rapid growth in the past 10 years because of concerns about environmental emissions from centralized power plants and the uncertainty of global energy supplies. These sources are pollution-free sources of abundant power. In addition, they generate power near the load centers, hence eliminating the need for running high voltage transmission lines through rural and urban landscapes [1,2].

According to recent works on fuel cell characteristics [3-5] and the specific properties of FCs, their output power response is delayed due to the processing time through subsidiary equipment and their slow internal electrochemical and thermodynamic characteristics. Therefore, in order to supply electric power to fluctuating loads by a hybrid FC system, an electric energy storage system is needed to compensate the gap between the output from the FC and the load, in addition to the collaborative load sharing [6]. Previous research works have shown that the hybridization of FC vehicles with batteries [2], with supercapacitors (ultracapacitors) [7], and with batteries/supercapacitors [8,9] provides cost, performance, and operational improvements, as well as fuel economy benefits that are attractive and should be considered by researchers

E-mail address: phtt@kmutnb.ac.th (P. Thounthong) 0142-0615/\$ - see front matter @ 2013 Elsevier Ltd. All rights reserved.

http://dx.doi.org/10.1016/j.ijepes.2013.07.033

The control problem (dc link stabilization) is important in many power electronic applications, such as robust control methods for unified power flow controller [10], control of solar power systems [11], and control for a wind energy conversion system [12]. Traditional methods to solve this problem are regularly based on a linearized model of the power converter and proportional-integral (PI) or proportional-integral-derivative (PID) feedback.

Control, robustness, stability, efficiency, and optimization of distributed generation systems remain an essential area of research. Recent work on controlling a FC/supercapacitor hybrid power plant is reported in [13], where a linear control using PI compensators was proposed for dc link stabilization. This work established a regularly used cascade controller structure for the supercapacitor current and dc bus voltage where the regulation of the supercapacitor current is contained inside the PI control for the dc bus voltage. Thus, design controller parameters basedon linear methods require a linear approximation, where this is dependent on the operating point. Because the switching model of the hybrid power plant is nonlinear, it is natural to apply model-based nonlinear control strategies that directly compensate for system nonlinearity without requiring a linear approximation. Studies of some nonlinear controllers for nonlinear systems have been proposed, such as nonlinear robust control of proton exchange membrane fuel cell by state feedback exact linearization [14], or nonlinear control for fuel cell/battery/ultracapacitor hybrid power sources [15]. However, more than 90% of industrial

<sup>\*</sup> Corresponding author. Tel.: +66 2 913 2500x3332; fax: +66 2 587 8255.

Nomenclature alternating current supercapacitor power reference (set-point) (W) PSCREF DC direct current maximum supercapacitor power (W)  $p_{SCMax}$ FC DC bus voltage (V) fuel cell UBus SC supercapacitor UFC fuel cell voltage (V) total capacitance at DC bus (F)  $C_{\mathrm{Bus}}$ supercapacitor voltage (V) total capacitance of supercapacitor module (F) DC bus energy (1) Csc EBus DC bus energy reference (set-point) (J) DC bus load current (A) EBusREF iLoad supercapacitor energy (J) supercapacitor energy reference (set-point) (J) total energy at DC bus and supercapacitor (J) fuel cell current (A) fuel cell current reference (set-point) (A) **I**FCREF ESCREF supercapacitor current (A)  $E_T$ supercapacitor current reference (set-point) (A) equivalent series resistance in fuel cell converter  $(\Omega)$ i<sub>SCREE</sub> TFC load power (W) equivalent series resistance in supercapacitor converter  $p_{Load}$ TSC fuel cell power (W)  $(\Omega)$ PEC fuel cell output power to DC bus (W) input variable vector PFCo fuel cell power reference (set-point) (W) maximum fuel cell power (W) state-variable vector PECREE output vector PFCMax supercapacitor power (W)  $\varphi(\cdot), \psi(\cdot), \phi(\cdot)$  smooth mapping functions Psc supercapacitor output power to DC bus (W)

controllers are still implemented based on linear control algorithms (PI or PID controllers), including the following advantages: clear functionality, applicability, and ease of use [16].

This paper presents a performance comparison between a proposed flatness-base control and a classical linear control for dc link stabilization of an FC/supercapacitor hybrid power source. It will provide a significant contribution to the field of multi-source systems, particularly in nonlinear power electronics applications. The flatness-based control of a FC/supercapacitor power plant will show good convergence of the dc-bus voltage regulation to its desired reference compared the classical PI controller, as studied in previous works [3,9,13]. There are no operating points and linearization models used in the proposed new control system. In Section 2, the FC and supercapacitor converter structure of multi-phase power converters is presented in detail, including a mathematic model of the power plant. The control laws based on the differential flatness property and linear PI control in Section 3 will be explained in detail. Simulation and experimental results will show the system performances of linear and nonlinear control laws. The summary and conclusions are presented in Section 4.

## 2. Fuel cell/supercapacitor hybrid power plant

## 2.1. System configuration studied

Normally, an FC system needs a boost dc/dc converter to adapt the FC output low voltage to the desired higher voltage level [17] and a storage device needs a bidirectional dc/dc converter (or two-quadrant converter) [18]. Nevertheless, a single converter will be limited when the power increases or for higher step-up ratios. That way, the use of paralleling power converters with the interleaved technique may offer better performance [19].

The power converter structure of the system studied in this paper is shown in Fig. 1. The FC converter is composed of 4-phase parallel boost converters, and the supercapacitor converter is composed of 4-phase parallel bidirectional converters (2-quadrant converters). These parallel connected converters, with interleaved switching technique, increase the power processing capability and availability of the power electronic system. Interleaved power conversion constitutes one of the most promising alternatives for the following advantages [19,20]:

(i) ripple cancellation both in the input and output waveforms to the maximum extent,

- (ii) a lower value of ripple amplitude and a high ripple frequency in the resulting input and output waveforms,
- (iii) improvement of the efficiency of the parallel connected converter system if a proper number of converters in the system are activated,
- (iv) fewer output capacitors is due to lower output-ripple current, which results in lower cost and lower power dissipation.

The prototype FC converter (1 kW) and the supercapacitor converter (2 kW) (refer to Fig. 1) were realized in the laboratory. The converter parameters and semiconductor components are detailed in Table 1.

For safety and high dynamics, the FC and supercapacitor converters are primarily controlled by inner current regulation loops, classically [13]. The current controls of these converters are similar to a basic current control of parallel converters. They can be easily realized by linear (PI) controllers [21] or nonlinear (sliding mode) current controllers [22]. To ensure system stability, the dynamics of the inner current regulation loops are also assumed to be much faster than those of the outer control loops [23]. These current control loops are supplied by two reference signals; the supercapacitor current reference  $i_{\text{SCREF}}$  and the FC current reference  $i_{\text{FCREF}}$ , generated by the control laws, are presented below.

## 2.2. Mathematical model

We consider that the FC and supercapacitor currents follow their reference values perfectly. Consequently,

$$i_{\text{FC}} = i_{\text{RCREF}} = \frac{p_{\text{FC}}}{v_{\text{FC}}} = \frac{p_{\text{FCREF}}}{v_{\text{FC}}} \tag{1}$$

$$i_{SC} = i_{SCREF} = \frac{p_{SC}}{v_{SC}} = \frac{p_{SCREF}}{v_{SC}}$$
 (2)

Then, the FC generator and the supercapacitor storage device function as controlled current sources. We consider here that there are only static losses in these converters, and  $r_{\rm FC}$  and  $r_{\rm SC}$  represent the static losses in the FC and supercapacitor converters, respectively.

The dc-bus capacitive energy  $E_{\rm Bus}$  and the supercapacitive energy  $E_{\rm SC}$  can be written as:

$$E_{\text{Bus}} = \frac{1}{2} C_{\text{Bus}} \nu_{\text{Bus}}^2 \tag{3}$$

P. Thounthong et al./Electrical Power and Energy Systems 54 (2014) 454-464

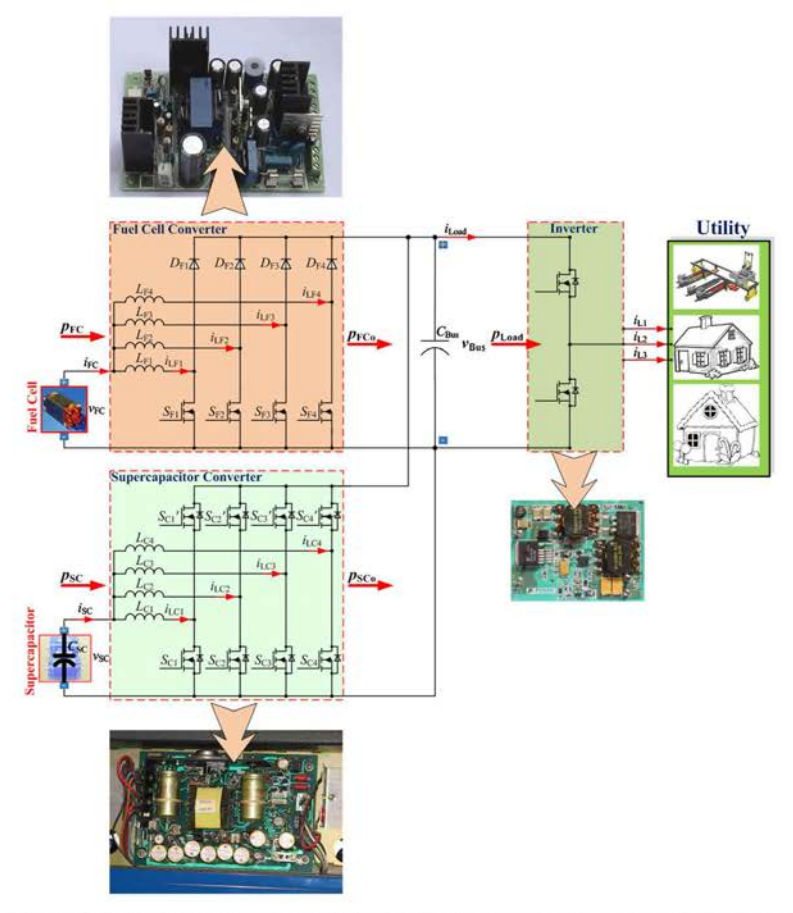


Fig. 1. Proposed circuit diagram of a distributed cogeneration system supplied by a fuel cell and supercapacitor, where  $p_{Load}$  (= $v_{Bus} \times i_{Load}$ ),  $p_{FC}$  (= $v_{FC} \times i_{FC}$ ),  $p_{SC}$  (= $v_{SC} \times i_{SC}$ ).  $p_{FCo}$  and  $p_{SCo}$  are the output powers to the DC link from the converters of fuel cell and supercapacitor, respectively.

Table 1
Converter parameters and semiconductor devices.

Fuel cell converter	
Inductors $L_{F1} = L_{F2} = L_{F3} = L_{F4}$	420 µH
MOSFETs $S_{F1} = S_{F2} = S_{F3} = S_{F4}$	IRFP264N: 250 V, 38 A
Diodes $D_{F1} = D_{F2} = D_{F3} = D_{F4}$	RURG3020: 200 V,
	30 A
Supercapacitor converter	
Inductors $L_{C1} = L_{C2} = L_{C3} = L_{C4}$	290 μΗ
MOSFETs	IRFP264N: 250 V, 38 A
$S_{C1} = S_{C2} = S_{C3} = S_{C4} = S'_{C1} = S'_{C2} = S'_{C}$	$S_{3} = S'_{C4}$

$$E_{SC} = \frac{1}{2}C_{SC}v_{SC}^2 \qquad (4)$$

The total electrostatic energy  $E_T$  stored in the dc-bus capacitor  $C_{\text{Bus}}$  and in the supercapacitor  $C_{\text{SC}}$  can also be written as:

$$E_T = \frac{1}{2} C_{Bus} v_{Bus}^2 + \frac{1}{2} C_{SC} v_{SC}^2$$
(5)

 $E_{T} = \frac{1}{2}C_{\text{Bus}}v_{\text{Bus}}^{2} + \frac{1}{2}C_{\text{SC}}v_{\text{SC}}^{2} \tag{5}$  As depicted in Fig. 1, the dc-bus capacitive energy  $E_{\text{Bus}}$  is given versus  $p_{\text{FCo}}$ ,  $p_{\text{SCo}}$ , and  $p_{\text{Load}}$  by the following differential equation:

$$\dot{E}_{\text{Bus}} = p_{\text{FCo}} + p_{\text{SCo}} - p_{\text{Load}}$$
 (6)

$$p_{\rm FCo} = p_{\rm FC} - r_{\rm FC} \left(\frac{p_{\rm FC}}{v_{\rm FC}}\right)^2 \tag{7}$$

$$p_{SCo} = p_{SC} - r_{SC} \left(\frac{p_{SC}}{v_{SC}}\right)^2 \tag{8}$$

$$p_{\text{Load}} = v_{\text{Bus}} \cdot i_{\text{Load}} = \sqrt{\frac{2E_{\text{Bus}}}{C_{\text{Bus}}}} \cdot i_{\text{Load}}$$
 (9)

$$p_{SC} = v_{SC} \cdot i_{SC} = \sqrt{\frac{2E_{SC}}{C_{SC}}} \cdot i_{SC}$$
 (10)

P. Thounthong et al. /Electrical Power and Energy Systems 54 (2014) 454-464

#### 3. Control algorithm

#### 3.1. Energy management

Several researchers have studied different topologies for the energy management of multi-power sources. Schaltz et al. [24] studied two energy-management strategies of an FC/battery/supercapacitor hybrid power source for vehicle applications. Feroldi et al. [25] studied control based on an efficiency map of an FC/supercapacitor hybrid power source for vehicle applications. Jiang et al. [26] studied control based on adaptive control with a state machine estimation of a FC/Li-Ion battery hybrid power source. Uzunoglu and Alam [27] studied control based on a wavelet-based load sharing algorithm of an FC/supercapacitor hybrid power source, and Thounthong et al. studied a regulated dc-bus voltage FC/supercapacitor hybrid source (based on a basic linear controller) [13], a FC/supercapacitor hybrid source (based on a fuzzy logic controller) [28], and an unregulated dc-bus voltage FC/battery hybrid source (based on a linear controller) [29]. Nevertheless, in these kinds of structures, the control, robustness, stability, efficiency, and optimization of fuel cell hybrid sources remain an essential area of research.

As recommended in [2,3], one must operate an FC with slow dynamics in order to prevent the fuel starvation phenomenon and thus improve its stack lifetime. The slow dynamics of an FC can be compensated by faster dynamics from storage devices. In contrast to batteries, supercapacitors have lower energy density but higher power density and provide very fast current charge/discharge cycles because of their low equivalent series resistance. Supercapacitors can provide more cycles than batteries and are well suited to very high dynamic cycles [30,31].

The energy management strategy based on dynamic classification aims at distributing the global power mission of the system (such as a fuel cell vehicle or uninterruptible power supply (UPS) or a fuel cell power plant) into the sources in such a way that each source is optimally used. According to the two points mentioned above, a fuel cell generator is controlled as a lower dynamic power source. A supercapacitor is a higher dynamic power source, which provides the micro-cycles and the fast dynamic power supply [13].

In this kind of system, as depicted in Fig. 1, there are two-voltage variables or two-energy variables to be regulated:

- $\bullet$  First, the dc bus voltage  $v_{\rm Bus}$  is the most important variable.
- Second, the supercapacitor voltage v<sub>SC</sub> (state-of-charge SOC) must be regulated.

Therefore, the basic principle of the proposed hybrid energy management lies in using the supercapacitors (the faster energy source) to supply the energy required to achieve the dc bus voltage regulation (or the dc bus energy regulation, called "DC link stabilization") [13]. Then, the fuel cell, although obviously the main energy source of the system, functions as the generator (with dynamic limitations) that supplies energy for both the dc bus capacitor  $C_{\text{Bus}}$  and the supercapacitors  $C_{\text{SC}}$  to keep them charged.

## 3.2. Nonlinear control of DC link stabilization

Differential flatness theory (nonlinear control) was first introduced by Fliess et al. [32]. This allowed an alternate representation of the system where trajectory planning and nonlinear controller design is clear-cut. The advantages of the differential flatness approach are that the trajectories of the system are estimated in a straightforward manner by the trajectories of a flat output and its derivatives without integrating any differential equation. These ideas have been used lately in a variety of nonlinear systems across various engineering disciplines including:

- · A process of stirred tank chemical reactor [33],
- Vehicle steering control [34]
- Control of a high-speed linear axis driven by pneumatic muscle actuators [35],
- Control of cathode pressure and oxygen excess ratio of a PEM fuel cell system [36],
- . Steering control of a two-level quantum system [37],
- Reactive power and dc voltage tracking control of a three-phase voltage source converter [38],
- · Control of open-channel flow in an irrigation canal [39],
- Current control for three phase three-wire boost converters
  [40]
- Design of a guidance algorithm for the hypersonic phase of a lifting-body vehicle [41],
  Control of a space robot with arbitrarily oriented joint axes and
- Control of a space robot with arbitrarily oriented joint axes and two momentum wheels at the base [42].

Then, this section gives a brief theory of differential flatness [32,43,44]. A system of ordinary differential equations (11) is said to be differentially flat if there exist variables (denoted by flat outputs, y) such that:

$$\dot{\mathbf{x}} = f(\mathbf{x}, \mathbf{u}) \tag{11}$$

$$\mathbf{x} = [x_1, x_2, \dots, x_n]^T; \quad \mathbf{x} \in \mathfrak{R}^n$$
 (12)

$$\mathbf{u} = [u_1, u_2, \dots, u_m]^T; \quad \mathbf{u} \in \Re^m$$
 (13)

$$\mathbf{y} = [y_1, y_2, \dots, y_m]^T; \quad \mathbf{y} \in \Re^m$$
 (14)

where  ${\bf x}$  is the state variables,  ${\bf u}$  is the vector of input (control) variables, and  $(n,m)\in \mathbb{N}.$ 

These variables are functions of the states, inputs and finite derivatives of the inputs of the form:

$$\mathbf{y} = \phi(\mathbf{x}, u, \dot{u}, \dots, u^{(\alpha)}) \tag{15}$$

where  $\alpha$  is a finite number of derivatives.

All the states and inputs can be expressed in terms of the flat outputs and their derivatives by equations of the type:

$$\mathbf{x} = \varphi(\mathbf{y}, \dot{\mathbf{y}}, \dots, \mathbf{y}^{(\beta)}) \tag{16}$$

$$\mathbf{u} = \psi(y, \dot{y}, \dots, y^{(\beta+1)}) \tag{17}$$

where  $\beta$  is a finite number of derivatives.

If the output variables of interest can be proven to be flat outputs  $\mathbf{y}$ , reference control design  $y_{REF}$  becomes straightforward. The dynamics of the resulting linear error dynamics can be specified (control law) [38,40].

$$0 = \left(y_i^{(\beta+1)} - y_{i,\text{REF}}^{(\beta+1)}\right) + K_\beta \left(y_i^\beta - y_{i,\text{REF}}^\beta\right) + \dots + K_0 (y_i - y_{i,\text{REF}}) \quad (18.1)$$

where  $K_{\beta},\ldots,K_{0}$  are the set of controller parameters. Then, there is no differential equation of the form:

$$0 = \zeta(y, \dot{y}, \dots, y^{(\delta)}) \tag{18.2}$$

where  $\delta$  (= $\beta$  + 1) is a finite number of derivatives

Note that the vector functions  $\phi(\cdot)$ ,  $\phi(\cdot)$ ,  $\psi(\cdot)$ , and  $\zeta(\cdot)$  are assumed to be smooth. The flat outputs  $\mathbf{y}$  and their derivatives provide an alternate representation of the system dynamics such that if the flat output profiles are known as a function of time, then one can obtain the profiles of all the system states and the corresponding inputs. This property is used to calculate the flat output trajectories, which are then mapped to the inputs  $\mathbf{u}$ . Clearly, an advantage of the differential flatness approach is that the trajectories of the system, i.e.  $\langle \mathbf{x}, \mathbf{u} \rangle$ , are estimated in a straightforward

manner by the trajectories of **y** and their derivatives without integrating any differential equations [37].

Based on the flatness control law introduced above, the dc-bus electrostatic energy  $E_{\rm Bus}$  stored in  $C_{\rm Bus}$  is assumed to be the flat output component. Thus, one defines a flat output  $y_1 = E_{\rm Bus}$ , a control variable  $u_1 = p_{\rm SCREF}$ , and a state variable  $x_1 = v_{\rm Bus}$ . From Eq. (3), the state variable  $x_1$  can be written as:

$$x_1 = \sqrt{\frac{2y_1}{C_{Bus}}} = \phi_1(y_1)$$
 (19)

From (6), the control variable  $u_1$  can be calculated from the flat output  $y_1$  and its time derivatives:

$$u_1 = 2 \cdot P_{\text{SCLimitted}} \cdot \left[ 1 - \sqrt{1 - \left( \frac{\dot{y}_1 + \sqrt{\frac{2y_1}{c_{\text{East}}}} \cdot \dot{t}_{\text{Load}} - p_{\text{FCo}}}{P_{\text{SCLimitted}}} \right)} \right]$$

$$= \psi_1(y_1, \dot{y}_1)$$
(20)

where

$$P_{\text{SCLimited}} = \frac{v_{\text{SC}}^2}{4r_{\text{SC}}}$$
 (21)

 $P_{\text{SCLimited}}$  is the limited maximum power from the supercapacitor converter.

It is apparent that  $x_1=\phi_1(y_1)$  and  $u_1=\psi_1(y_1,\dot{y}_1)$  correspond to (16) and (17). Consequently, the mathematical model (the reduced order model) of the hybrid system can be considered as a flat system.

A desired reference for the dc-bus energy is represented by  $y_{1REF}$ . A linearizing feedback control law achieving an exponential asymptotic tracking of the trajectory is given by the following expression [45]:

$$(\dot{y}_1 - \dot{y}_{1REF}) + K_{11}(y_1 - y_{1REF}) + K_{12} \int_0^t (y_1 - y_{1REF}) d\tau = 0$$
 (22)

where the set of controller parameters  $(K_{11}, K_{12})$  is chosen such that the roots of the closed loop characteristic polynomial, in the complex variable s:

$$p(s) = s^2 + \lambda_1 s^1 + \lambda_0 \tag{23}$$

is a Hurwitz polynomial.

Obviously, the tracking error,  $e_1 = y_1 - y_{1REF}$ , satisfies:

$$e_1 + K_{11}\dot{e}_1 + K_{12}e_1 = 0 (24)$$

An optimum choice of the design controller parameters is obtained by matching the characteristic polynomial, p(s), to a desired characteristic polynomial, with pre-specified root locations. We may set as a desired characteristic polynomial:

$$p(s) = s^2 + 2\zeta \omega_n s + \omega_n^2 \tag{25}$$

$$K_{11} = 2\zeta \omega_n \tag{26}$$

$$K_{12} = \omega_n^2 \tag{27}$$

where  $\zeta$  and  $\omega_n$  are the desired dominant damping ratio and natural frequency.

Substituting the expression for  $\dot{y}_1$  into (20) gives the equation for the closed-loop static state feedback supercapacitor power:

$$\begin{split} \mu_1 &= 2 \cdot P_{\text{SCLimited}} \\ &\cdot \left[ 1 - \sqrt{1 - \left( \frac{(\dot{y}_{\text{IREF}} - K_{11}e_1 - K_{12} \int_0^\epsilon e_1 d\tau) + p_{\text{Load}} - p_{\text{FCO}}}{P_{\text{SCLimited}}} \right)} \right] \\ &= p_{\text{SCREF}} \end{split}$$

The control system is stable for  $K_{11}, K_{12} > 0$  ( $\zeta, \omega_n > 0$ ). However, based on the power electronic constant switching frequency  $\omega_S$  and the cascade control structure, the outer control loop (here, the dc-bus energy control) must operate at a cut-off frequency  $\omega_E \ll \omega_P$  (a cut-off frequency of the supercapacitor power loop)  $\ll \omega_S$ . Once the flat outputs are stabilized, the whole system is stable because all the variables of the system are expressed in terms of the flat outputs.

Thus, the nonlinear control law of the dc link stabilization detailed above is portrayed in Fig. 2. The nonlinear control law generates a supercapacitor power reference  $p_{SCREF}$ . This signal is limited to a converter maximum power  $p_{SCMin}$  and a minimum power  $p_{SCMin}$ . in which  $p_{SCMin} \in p_{SCMin}$  by  $p_{SCMin} \in p_{SCMin}$  is then divided by the measured supercapacitor voltage  $v_{SC}$ . The supercapacitor power is limited to maintain the supercapacitor current within the nominal values; the reference power is set to zero when the supercapacitor voltage is outside the interval  $[V_{SCMin}, V_{SCMax}]$ , as presented in the block "SuperC Current Limitation Function" [13]. This results in a supercapacitor current reference  $i_{SCREF}$ .

### 3.3. Linear control of DC link stabilization

In order to compare the performance of the flatness-based control, a traditional linear PI control method presented in [13] is also implemented on the hybrid test stand. Here, we briefly review this approach. A desired reference for the dc-bus energy is represented by  $y_{1REF}$ . A linear feedback PI control law is given by the following expression:

$$p_{\text{SCREF}} = K_P(y_{1\text{RFF}} - y_1) + K_I \int_0^t (y_{1\text{RFF}} - y_1) d\tau$$
 (29)

where  $K_P$ ,  $K_I$  are the set of controller parameters. Note that, in power electronics applications, the system composes of many spike signals coming from the high frequency switching of power switching devices. If using a PID controller, differentiation (D) increases the high-frequency gain. A pure differentiator is not proper or causal. When a spike change (or a noisy environment) of the disturbance occurs, differentiation results in a theoretically infinite control signal, called "chaos phenomenon". A filter to the differentiator may be added [46] in consideration of high frequency noise suppression. This is the reasons that in power electronics applications a PI controller (a PID controllers that the derivative part omitted or switched off) is widely chosen instead of a PID controller [11,12,47].

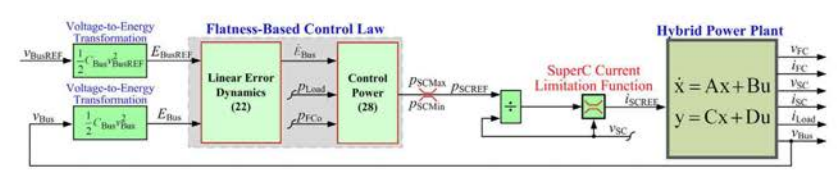


Fig. 2. DC link stabilized fuel cell/supercapacitor hybrid source based on differential flatness control law.

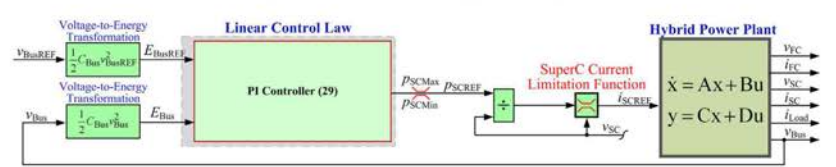


Fig. 3. DC link stabilized fuel cell/supercapacitor hybrid source based on linear Pl control law.

Therefore, because the supercapacitor current loop is much faster than the dc link voltage loop (so that it can be considered as a pure unity gain, refer to (6)), the open loop transfer function associated with the dc link voltage regulation can be written as

$$\frac{E_{\text{Bus}}(s)}{E_{\text{Bus}\text{REF}}(s)} = \underbrace{(K_P + \frac{K_I}{s})}_{\text{PL}} \cdot \underbrace{\frac{1}{s}}_{\text{ps}} \cdot \underbrace{\frac{1}{T_p s + 1}}_{\text{ps}}$$
(30)

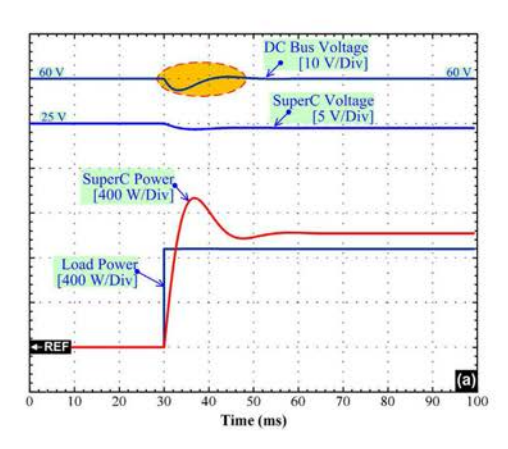
where  $T_P$  is the time constant of an equivalent first-order delay of the supercapacitor power regulation loop (or the supercapacitor current regulation loop). Thus, the linear control law of the dc link stabilization detailed above is portrayed in Fig. 3. It is similar to the nonlinear control law (refer to Fig. 2), where the PI controller also generates a supercapacitor power reference  $p_{SCRFE}$ .

## 3.4. Performance comparison between linear control and nonlinear control law for DC link stabilization

In order to compare the performance of the flatness-based control and the linear PI control laws, the simulation and test bench were implemented. Simulations with Matlab/Simulink were performed using a reduced-order model of the power plant, as portrayed in Fig. 1. The parameters of the power plant were  $v_{\rm BusREF}$  = 60 V,  $C_{\rm Bus}$  = 7800  $\mu$ F;  $r_{\rm FC}$  = 0.13  $\Omega$ ;  $r_{\rm SC}$  = 0.08  $\Omega$ ; and  $T_P$  = 2.2 ms. The supercapacitor module (100 F, 32 V, based on Maxwell Technologies Company) was obtained by means of 12 cells BCAP1200 (capacitance: 1200 F; maximum voltage: 2.7 V) connected in series, as shown in Fig. A2.

The nonlinear controller gains used were  $K_{11}$  = 450 rad s<sup>-1</sup> and  $K_{12}$  = 22,500 rad<sup>2</sup> s<sup>-2</sup>, so that the system damping ratio  $\zeta$  was equal to 1.5, and the natural frequency  $\omega_n$  was equal to 150 rad s<sup>-1</sup>. As a result, the cutoff frequency  $(\omega_E)$  of the closed-loop dc-bus energy was equal to 60 rad s<sup>-1</sup>, which is lower than the cutoff frequency  $(\omega_P)$  of the supercapacitor power loop of 600 rad s<sup>-1</sup> ( $T_P$  = 2.2 ms), so that the system was stable.

Fig. 4 presents waveforms that are obtained during the large load step. They show the dc bus voltage (the state  $x_1$ , representing the flat output  $y_1$ ), the supercapacitor voltage, the load power, and the supercapacitor power. The initial state is in no-load power, and the supercapacitor storage device is full of charge, i.e., the supercapacitor voltage = 25 V; as a result, the supercapacitor power is zero. The simulation results in Fig. 4(a) and the real test bench results in Fig. 4(b) were carried out in order to compare the responses to a large load step from 0 W to 880 W at t = 30 ms. The results reveal that, corresponding to the dynamics (25) of the observation error, the dynamic response is affected by this kind of outsized perturbation. The small oscillations in  $v_{\rm Bus}$  are due to a large proportional gain  $K_{12}$  and the vast load step. The value of  $K_{12}$  can be reduced to attenuate the oscillations; however, this leads to a slower transition. The simulation also results show excellent concurrence with the experimental data. It should be noted here that the perfect large power load step is very difficult to perform, as can be seen in Fig. 4(b). One can also estimate that the static losses  $(r_{SC})$  in the supercapacitor converter are around 120 W in Fig. 4(b). Therefore, the present mathematical model of the hybrid power plant



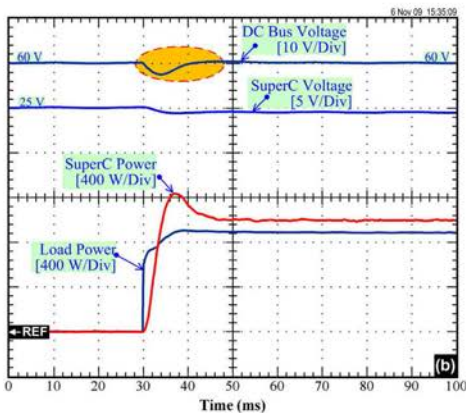


Fig. 4. Flatness-based control law. Response to a large load step from 0 W to 880 W at t=30 ms. (a) Simulation results. (b) Experimental results.

precisely predicts the dynamics of the system when compared to experiment; consequently, the simulation model is a valuable tool for control algorithm validation.

Finally, in order to give a reasonable comparison between the methods, the parameters of the linear controller  $K_P$  and  $K_I$  were tuned to obtain the best possible performance, and this result is compared to the flatness-based control. In this paper, the symmetrical optimum (SO) is studied [48], [49]. A SO design criterion obtains a controller that forces the frequency response of the system as close as possible to that for low frequencies. The method has the advantage of maximizing the phase margin. As phase margin is maximized for given frequency, the system can tolerate

459

more delays, which is important for systems having delays. This method optimizes the control system behavior with respect to disturbance input. The method has well established tuning rules and has good disturbance rejection. The resulting performance gives an overshoot of around 43%, settling time around 16.3- $T_p$  and a phase margin of 30–60°. Then, by using the SO method,  $K_P$  = 459 W J<sup>-1</sup> and  $K_I$  = 40,000 W (J s)<sup>-1</sup>, so that the desired phase margin is equal to 40°.

Figs. 5 and 6 show simulation and experimental results obtained for both controllers during the large load step. The flatness-based control shows good convergence of the dc bus voltage regulation to its desired reference of 60 V. Although dynamic response of the linear control law could be improved relative to that shown in the figures, this enhancement came at the expense of a reduced stability margin. From these results, we conclude that the flatness-based control provides better performance than the classical PI controller.

Note that, for the specification of the voltage regulation, the dc bus voltage sag is about 5% for a step load change from light load to  $\frac{3}{4}$  of nominal load. The dc bus voltage regulation based on the differential flatness approach could be reduced the dc bus voltage sag to 2% or lower by tuning the nonlinear controller gains ( $K_{11}$  and  $K_{12}$ ). In this study,  $K_{11}$  = 450 rad s<sup>-1</sup> and  $K_{12}$  = 22,500 rad² s<sup>-2</sup>, so that the system damping ratio  $\zeta$  was equal to 1.5, and the natural frequency  $\omega_n$  was equal to 150 rad s<sup>-1</sup>. In order to obtain the higher dynamics or lower voltage drop, the natural frequency  $\omega_n$  may be increased. Although lower voltage sag could be improved by increasing the defined natural frequency  $\omega_n$ , this enhancement came at the expense of a reduced stability margin.

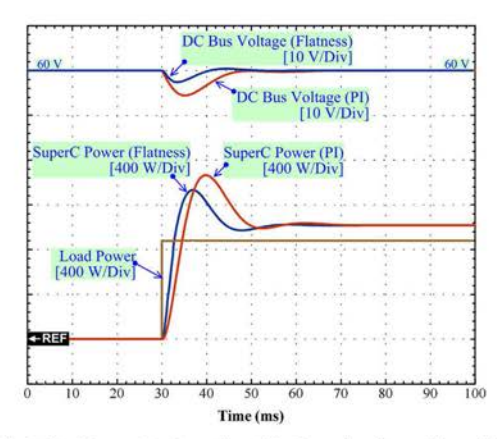
### 3.5. Charging supercapacitor

Again, based on the flatness-base control, we consider the total electrostatic energy  $E_T$  stored in the dc bus capacitor  $C_{\text{Bus}}$  and the supercapacitor  $C_{\text{SC}}$  as a flat output variable  $y_2$ ; refer to (5),

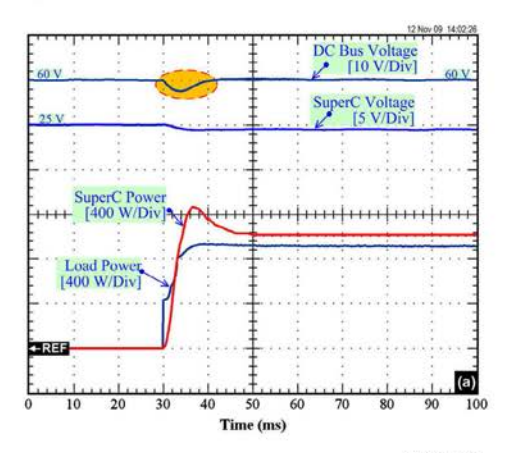
$$y_2 = E_7 = E_{Bus} + E_{SC} = \frac{1}{2}C_{Bus}v_{Bus}^2 + \frac{1}{2}C_{SC}v_{SC}^2$$
 (31)

Thus, one defines a control variable  $u_2 = p_{FCREF}$ , and a state variable  $x_2 = v_{SC}$ . From (4), the state variable  $x_2$  can be written as:

$$x_2 = \sqrt{\frac{2(y_2 - y_1)}{C_{SC}}} = \varphi_2(y_1, y_2), \tag{32}$$



**Fig. 5.** Simulation results: Comparison of the flatness-based control law with a linear PI control law. Response to a large load step from 0 W to 880 W at t = 30 ms.



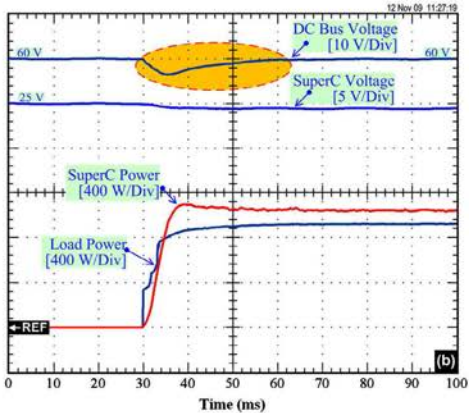


**Fig. 6.** Experimental results: Comparison of the flatness-based control law with a linear PI control law. Response to a large load step from 0 W to 920 W at t = 30 ms. (a) Flatness-based control law. (b) Linear PI control law.

From (6), the control variable  $u_2$  can be calculated from the flat output  $y_2$  and its time derivatives:

$$u_{2} = 2p_{\text{FCLimitted}} \cdot \left[ 1 - \sqrt{1 - \left( \frac{\dot{y}_{2} + \sqrt{\frac{2y_{1}}{c_{\text{bas}}}} \cdot \dot{i}_{\text{Load}}}{p_{\text{FCLimitted}}} \right)} \right]$$

$$= \psi_{2}(y_{1}, \dot{y}_{2}) \tag{33}$$

where

$$P_{\text{FCLimited}} = \frac{v_{\text{FC}}^2}{4r_{\text{FC}}}$$
(34)

 $P_{\rm FCLimited}$  is the limited maximum power from the fuel cell converter.

It is apparent that  $x_2 = \varphi_2(y_1, y_2)$  and  $u_2 = \psi_2(y_1, \dot{y}_2)$  correspond with (16) and (17). Consequently, the mathematical model (the reduced order model) of the hybrid system can be considered as a flat system.

Based on the flatness control law for the total energy regulation (or the supercapacitor energy regulation), a desired reference for the total energy is represented by  $y_{\rm 2REF}$ . Since the supercapacitor energy storage has an enormous size capacity and the supercapac-

P. Thounthong et al./Electrical Power and Energy Systems 54 (2014) 454-464

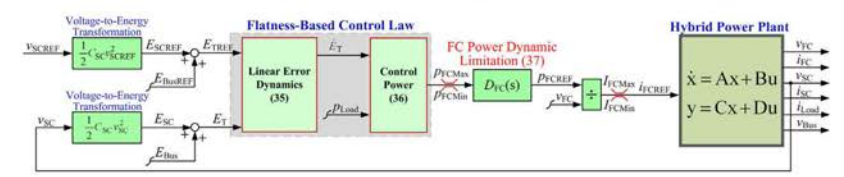


Fig. 7. Supercapacitor charging based on differential flatness-based control law.

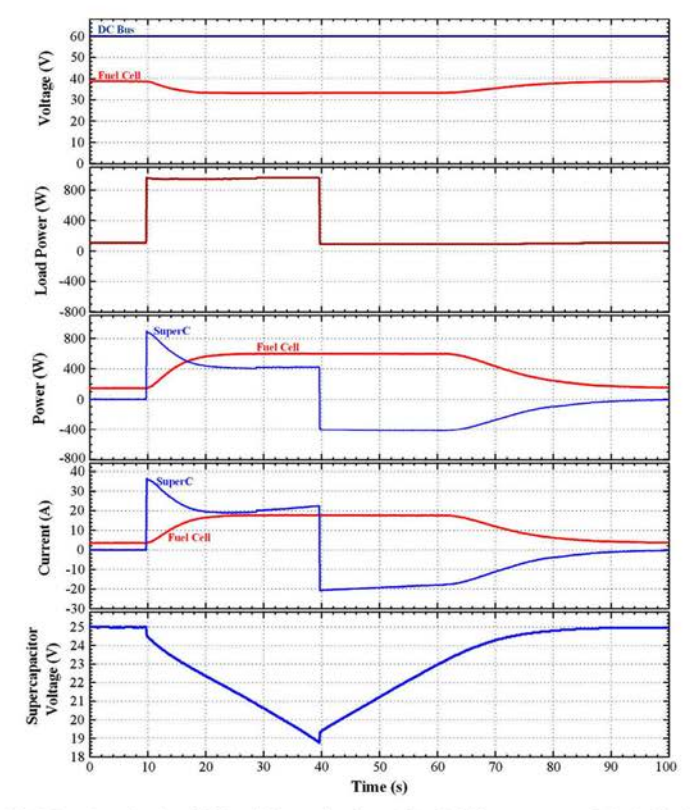


Fig. 8. Experimental results of differential flatness-based control law: hybrid source response during load cycle.

itor energy is defined as a slower dynamic variable than the dc-bus energy variable, the total energy control law is defined as:

$$\dot{y}_2 - \dot{y}_{2REF} + K_{21}(y_2 - y_{2REF}) = 0 ag{35}$$

Substituting the expression for  $\dot{y}_2$  into (33) gives the equation for the closed-loop static state feedback fuel cell power

$$e = 2p_{\text{FCLimited}}$$

$$= \left[1 - \sqrt{1 - \left(\frac{\dot{y}_{\text{2REF}} + K_{21}(y_{\text{2REF}} - y_2) + p_{\text{Load}}}{1 - y_{\text{Load}}}\right)}\right]$$

$$= p_{\text{FCREF}} \tag{36}$$

with  $K_{21} > 0$  enforcing tracking convergence.

Fig. 7 depicts the supercapacitor charging algorithm. The total energy control law generates the FC power reference  $p_{\text{FCREF}}$ . It must

be limited in level, within an interval maximum  $p_{\text{FCMax}}$  (corresponding to a rated power of the FC, so  $p_{\text{FCMax}} \leqslant p_{\text{FCLimited}}$ ) and minimum  $p_{\text{FCMin}}$  (set to 0 W) and limited in dynamics, which enables the safe operation of the FC with respect to the constraints that are associated with the FC (the prevention of the fuel starvation phenomenon in the FC stack [10]). Here, the second order delay  $D_{\text{FC}}(s)$  is selected as the FC power dynamic limitation.

$$D_{FC}(s) = \frac{1}{\left(\frac{s}{\omega_{s1}}\right)^2 + \frac{2\zeta_1 s}{\omega_{s1}} + 1}$$
(37)

where  $\omega_{n1}$  and  $\zeta_1$  are the regulation parameters. Then, the fuel cell power reference  $p_{\text{FCREF}}$  is divided by the measured fuel cell voltage  $v_{\text{FC}}$ . This results in a fuel cell current reference  $i_{\text{FCREF}}$ . For safety, the fuel cell current reference  $i_{\text{FCREF}}$  must be limited in level within an

interval [maximum fuel cell current  $I_{\rm FCMax}$  (corresponding to a fuel cell rated current), minimum FC current  $I_{\rm FCMin}$  (set to 0 A)].

It should be noted here that, for charging the supercapacitor, only the nonlinear control law has been studied, because the differential flatness-based control law shows better performance than the linear control approach.

3.6. System performance of hybrid power source control based on flatness control

The small-scale fuel cell/supercapacitor hybrid power plant implemented in the laboratory is described in Appendix A. For the dc-bus voltage stabilization, the control system parameters are  $\nu_{\rm BusrREF}=60$  V;  $C_{\rm Bus}=7800~\mu{\rm F};~r_{\rm FC}=0.13~\Omega;~r_{\rm SC}=0.08~\Omega;~T_p=2.2~{\rm ms};~V_{\rm SCMax}=32$  V;  $V_{\rm SCMin}=15$  V;  $I_{\rm SCRated}=150$  A;  $K_{11}=450~{\rm rad~s^{-1}};~{\rm and}~K_{12}=22,500~{\rm rad^2~s^{-2}}.~{\rm For}~{\rm the~supercapacitor~voltage~regulation},~{\rm the~control~system~parameters~are~}\nu_{\rm SCREF}=25$  V (full of charge);  $C_{\rm SC}=100$  F;  $K_{\rm 21}=0.1~{\rm JW^{-1}};~p_{\rm FCMax}=600~{\rm W};~p_{\rm FCMin}=0~{\rm W};~{\rm and~}I_{\rm FCMax}=46~{\rm A}~{\rm (rated)},~I_{\rm FCMin}=0~{\rm A}.~{\rm The~parameters~for~the~full~cell~power~dynamic~delay~are~}\omega_{\rm n1}={\rm rad~s^{-1}~and~}\zeta_1=1.~{\rm This~value~was~experimentally~determined~to~be~the~highest~power~slope~of~our~fuel~cell~system,~where~no~fuel~starvation~occurs.~It~must~be~noted~here~that,~for~the~small-test~bench,~the~FC~maximum~power~}p_{\rm FCMax}~{\rm was~set~at~600~W};~in~fact,~the~rated~fuel~cell~power~considered~here~is~1200~W.}$ 

For simulation, the model is tuned to the real system of the 1.2-kW Nexa PEMFC (refer to Fig. A2), using experimental data

 $V_{\rm FC}$  = f( $I_{\rm FC}$ ) and taking 50 operating points to fit the polarization curve (polynomial curve fitting) in a least-squares sense. The stack voltage versus current is governed by the following equation:

$$V_{FC} = a_{6FC}I_{FC}^6 + a_{5FC}I_{FC}^5 + a_{4FC}I_{FC}^4 + a_{3FC}I_{FC}^3 + a_{2FC}I_{FC}^2 + a_{1FC}I_{FC} + a_{0FC}I_{FC}$$
+  $a_{0FC}I_{FC}I_$ 

where  $a_{\rm GFC}$  =  $5.5991 \times 10^{-8}$ ;  $a_{\rm SFC}$  =  $-7.8814 \times 10^{-6}$ ;  $a_{\rm 4FC}$  =  $4.2503 \times 10^{-4}$ ;  $a_{\rm 3FC}$  = -0.0114;  $a_{\rm 2FC}$  = 0.1664;  $a_{\rm 1FC}$  = -01.6023; and  $a_{\rm 0FC}$  = 42.62.

Figs. 8 and 9 present waveforms that are obtained during the load cycle: experimentation and simulation. They show the dc bus voltage (the state variable  $x_1$ , representing the flat output  $y_1$ ), the FC voltage, the load power, the supercapacitor power, the FC power, the supercapacitor current, the FC current, and the supercapacitor voltage (the state variable  $x_2$ , or the supercapacitor state-of-charge).

The initial state has a load power = 100 W, and the supercapacitor storage device is full of charge, i.e.,  $v_{SC} = 25$  V; as a result, the supercapacitor power is zero, and the FC power is equal to 100 W for the load power demanded. At t = 10 s, the load power steps to a constant value of 1000 W; synchronously, the final FC power increases with a limited slope (second order dynamics) to a limited maximum power of 600 W. Thus, the supercapacitor, which supplies most of the transient power that is required during stepped load, remains in a discharge state after the stepped load

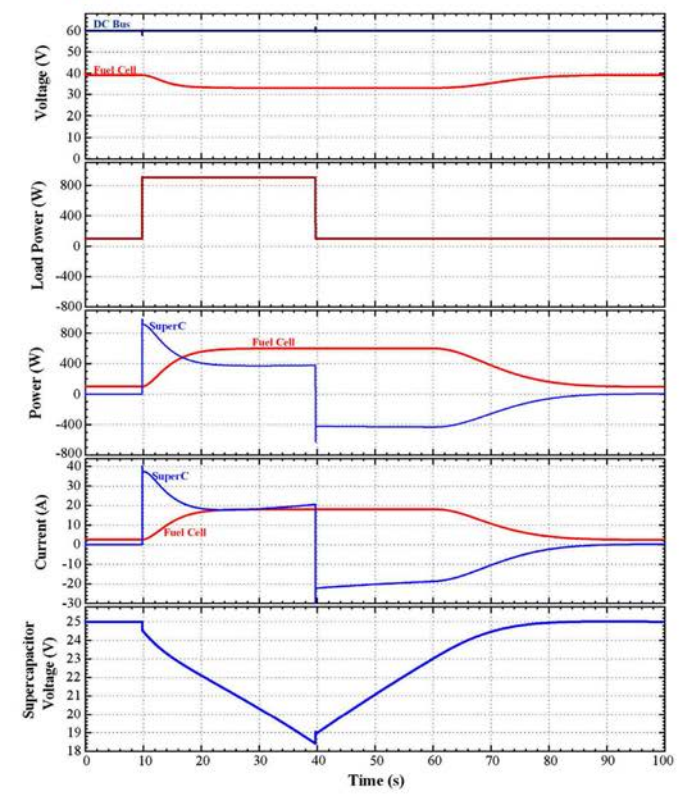


Fig. 9. Simulation results of differential flatness-based control law: hybrid source response during load cycle.

because the steady-state load power (1000 W) is greater than the FC limited maximum power (600 W)

Subsequently, at t = 40 s, the load power steps from 1000 W to 100 W. As a result, the supercapacitor changes its state from discharging to charging, demonstrating the three phases. First, the FC supplies its limited maximum power of 600 W for driving the load and for charging the supercapacitor. Second, at t = 62 s( $v_{SC}$  = 23.2 V), the supercapacitor is nearly fully charged at 25 V, which then reduces the charging power. Third, at t = 90 s, the supercapacitor is fully charged, and the supercapacitor charging power is zero. Finally, the FC supplies the constant load power of 100 W.

One can observe that the dc-bus voltage waveform is stable during the constant load power, the large positive load step, and the large negative load step, which is of major importance when employing supercapacitors to improve the dynamic performance of the whole system using the differential flatness-based control

#### 4. Conclusion

The key contribution of this paper is to study two dc link stabilization methods (linear and nonlinear) for the control of fuel cell/ supercapacitor power plants. The prototype power plant studied was composed of a PEMFC system (the Nexa Ballard FC power generator: 1.2 kW, 46 A) and a supercapacitor module (100 F, 32 V, based on Maxwell Technologies Company). The low voltage dc bus considered here was 60 V. Simulation (by Matlab/Simulink) and experimental results demonstrated the comparisons. The present mathematical model of the hybrid power plant precisely predicts the dynamics of the system when compared to experimental results; accordingly, the simulation model is an essential tool for control algorithm corroboration.

Differential flatness-based control of a FC/supercapacitor power plant of the load rejection transient offers superior voltage response, with smaller voltage dip and shorter recovery time, regardless of the voltage reference setting. This is frequently cited advantage of the nonlinear flatness control [38],[40]. However, the PI controller, being a standard industrial controller solution at present, will continue to be compared to various novel forms of voltage controllers that will emerge in the future (including fuzzy flatness controllers). It is important that, in such cases, a detailed comparative analysis of the system performance is always performed. Comparison based on a single operating point or a single transient is more than obviously insufficient.

However, the flatness-based control requires a load current measurement to estimate the load power in order to obtain the differential flatness property. For the linear control, there is no load current measurement. For future work, a load observer will be used to avoid the measurement of the load current.

## Acknowledgments

This work was supported in part by the research program in cooperation with the Thai-French Innovation Institute (TFII), King Mongkut's University of Technology North Bangkok (KMUTNB) with Université de Lorraine, and in part by the Thailand Research Fund (TRF) and Faculty of Technical Education (Research Grant for Mid-Career University Faculty) under Grant RSA5580009

## Appendix A. Test bench description of fuel cell/supercapacitor

The small-scale test bench of the hybrid power plant was implemented in our laboratory, as presented in Fig. A1. The FC system used in this effort was a PEMFC system (1.2 kW, 46 A, based on

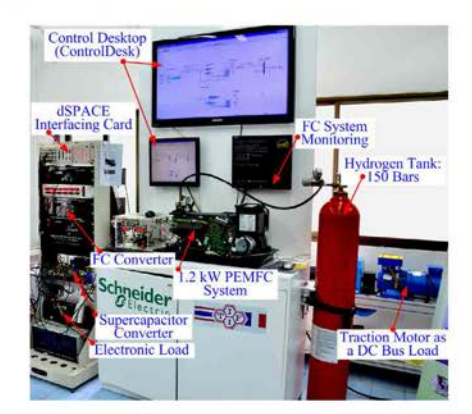


Fig. A1. Experimental setup of the fuel cell/supercapacitor hybrid power plant.



Fig. A2. Supercapacitor module (100 F. 32 V) used in the test bench.

Ballard Power Systems Company). It was supplied with pure hydrogen with a regulated pressure of 10 bars from bottles under a pressure of 150 bars and with clean and dry air from a compressor. The supercapacitor module (100 F, 32 V, based on Maxwell Technologies Company) was obtained by means of 12 BCAP1200 cells (capacitance: 1200 F; maximum voltage: 2.7 V) connected in series, as shown in Fig. A2

Measurements of the FC current  $i_{FC}$ , the supercapacitor current  $i_{
m SC}$ , the load current  $i_{
m Load}$ , the dc bus voltage  $v_{
m Bus}$ , the FC voltage  $v_{
m FC}$ , and the supercapacitor voltage  $v_{\rm SC}$  were carried out by means of zero-flux Hall effect sensors. The FC and supercapacitor current regulation loops were realized with analog circuits to function at a high bandwidth. The control loops, which generate current references  $i_{FCREF}$  and  $i_{SCREF}$ , were implemented in the real time card dSPACE DS1104, through the mathematical environment of Matlab-Simulink, with a sampling frequency of 25 kHz.

## References

- [1] Dursun E, Kilic O. Comparative evaluation of different power man Dursun E, Kilic O. Comparative evaluation of different power management strategies of a stand-alone PV/Wind/PEMFC hybrid power system. Int J Electr Power Energy Syst 2012;34:81–9.
   Zhan Y, Wanga H, Zhu J. Modelling and control of hybrid UPS system with backup PEM fuel cell/battery. Int J Electr Power Energy Syst 2012;43:1322–31.
   Thounthong P, Davat B, Raël S, Sethakul P. Fuel starvation: analysis of a PEM fuel cell system. IEEE Ind Appl Mag 2009;15:52–9.

#### P. Thounthong et al./Electrical Power and Energy Systems 54 (2014) 454-464

464

- Erdinc O, Vural B, Uzunoglu M. A wavelet-fuzzy logic based energy management strategy for a fuel cell/battery/ultra-capacitor hybrid vehicular power system. J Power Source 2009;194:369–80.
   Bizon N. A new topology of fuel cell hybrid power source for efficient operation and high reliability. J Power Source 2011;196:3260–70.
   Andújar JM, Segura F, Durán E, Renteria LA. Optimal interface based on power electronics in distributed generation systems for fuel cells. Renew Energy 2011;28-2750–70.

- 2011;36:2759-70.

  [7] Rodatz P, Paganelli G, Sciarretta A, Guzzella L. Optimal power management of an experimental fuel cell/supercapacitor-powered hybrid vehicle. Control Eng Pract 2005;13:41-53.

  [8] Li Q, Chen W, Li Y, Liu S, Huang J. Energy management strategy for fuel cell/battery/ultracapacitor hybrid vehicle based on fuzzy logic. Int J Electr Power Energy Syst 2012;43:514-25.

  [9] Thounthong P, Rael S, Davat B. Energy management of fuel cell/battery/supercapacitor hybrid power source for vehicle applications. J Power Source 2009;193:376-85.

  [10] Taher SA, Hemmati R, Abdolalipour A, Akbari S. Comparison of different robust control methods in design of decentralized UPFC controllers. Int J Electr Power Energy Syst 2012;43:173-84.

  [11] Ramasamy M, Thangavel S. Photovoltaic based dynamic voltage restorer with

- Energy Syst 2012;43:173–84.

  [11] Ramasamy M, Thangavel S, Photovoltaic based dynamic voltage restorer with power saver capability using PI controller. Int J Electr Power Energy Syst 2012;36:51–9.

  [12] Mesemanolis A, Mademlis C, Kioskeridis I. High-efficiency control for a wind energy conversion system with induction generator. IEEE Trans Energy Convers 2012;27(4):958–67.

  [13] Thounthong P, Rael S, Davat B. Analysis of supercapacitor as second source based on fuel cell power generation. IEEE Trans Energy Convers 2009;24:247–55.

  [14] Li Q, Chen W, Wang Y, Jia J, Hanc M, Nonlinear robust control of proton exchange membrane fuel cell by state feedback exact linearization. J Power Source 2009;194:338–48.

  [15] Bizon N, Nonlinear control of fuel cell hybrid power sources: Part I voltage control. Appl Energy 2011;88:2559–73.

- [15] Bizon N. Nonlinear control of fuel cell hybrid power sources: Part I voltage control. Appl Energy 2011;88:2559–76.
  [16] Ang KH, Chong G, Li Yun, PID control system analysis, design, and technology. IEEE Trans Control Syst Technol 2005;13(4):559–76.
  [17] Segura F, Andújar JM. Power management based on sliding control applied to fuel cell systems: a further step towards the hybrid control concept. Appl Energy 2012;99:213–25.
  [18] Erdinc O, Uzunoglu M. Recent trends in PEM fuel cell-powered hybrid systems: investigation of application areas, design architectures and energy management approaches. Renew Sustain Energy Rev 2010;14:2874–84.
  [19] Thounthong P, Pierfederici S. A new control law based on the differential flatness principle for multiphase interleaved DC—DC converter. IEEE Trans Circ Syst II Express Briefs 2010;57:903–7.
  [20] Shahin A, Huang B, Martin JPh. Pierfederici S. Davat B, New non-linear control
- (20) Shahin A, Huang B, Martin JPh, Pierfdedrici S, Davat B. New non-linear control strategy for non-isolated DC/DC converter with high voltage ratio. Energy Convers Manage 2010;51:56–63.
   [21] Pérez M, Ortega R, Espinoza JR. Passivity-based PI control of switched power
- [21] Pérez M, Ortega R, Espinoza JR. Passivity-based PI control of switched power converters. IEEE Trans Control Syst Technol 2004;12:881–90.
  [22] Thounthong P, Pierfederici S, Martin J-Ph, Hinaje M, Davat B. Modeling and control of fuel cell/supercapacitor hybrid source based on differential flatness control. IEEE Trans Veh Technol 2010;56(6):2700–10.
  [23] Mudannayake CP, Rahman MF. Future automotive 42-V powernet application. IEEE Ind Appl Mag 2009;15:14–25.
  [24] Schaltz E, Khaligh A, Rasmussen PO. Influence of battery/ultracapacitor energy-storage sizing on battery lifetime in a fuel cell hybrid electric vehicle. IEEE Trans Veh Technol 2009;58:3882–91.
  [25] Feroldi D, Serra M, Riera J. Energy management strategies based on efficiency map for fuel cell hybrid vehicles. J Power Source 2009;190:387–401.
  [26] Jiang Z, Gao L, Dougal RA. Adaptive control strategy for active power sharing in hybrid fuel cell/battery power sources. IEEE Trans Energy Convers 2007;29:22:507–15.

- 2007:22:507-15.

- [27] Uzunoglu M, Alam MS. Modeling and analysis of an FC/UC hybrid vehicular power system using a novel-wavelet-based load sharing algorithm. IEEE Trans Energy Convers 2008;23:263–72.
- Energy Convers 2008;23:263–72.

  [28] Vural B, Boynuegri AR, Nakir I, Erdinc O, Balikci A, Uzunoglu M, et al. Fuel cell and ultra-capacitor hybridization: a prototype test bench based analysis of different energy management strategies for vehicular applications. Int J Hydrogen Energy 2019;35:161–71.

  [29] Thounthong P, Rael S, Davat B. Control algorithm of fuel cell and batteries for distributed generation system. IEEE Trans Energy Convers 2008;23:148–55.

  [30] Omar R, Rahim NA. Voltage unbalanced compensation using dynamic voltage restorer based on supercapacitor. Int J Electr Power Energy Syst 2012;43:573–81.

  [31] Das DCh, Roy AK, Sinha N, GA based frequency controller for solar themal diesel-wind hybrid energy generation/energy storage system. Int J Electr

- dissel-wind hybrid energy generation/energy storage system. Int J Electr
  Power Energy Syst 2012;43:262–79.

  [32] Fliess M, Lévine J, Martin Ph, Rouchon P, Flatness and defect of nonlinear
  systems: introductory theory and examples. Int J Control 1995;61:1327–61.

  [33] Guay M. On the linearizability of nonisothermal continuous stirred-tank
  reactors. Automatica 2002;38:269–78.

- [34] Villagra J, Novel BA, Mounier H, Pengov M. Flatness-based vehicle steering
- [24] Yunogra J. Novei BA. Mounier H. Pengov M. Flatness-based vehicle steering control strategy with SDRE feedback gains tuned via a sensitivity approach. IEEE Trans Control Syst Technol 2007;15:554-64.
   [35] Aschemann H. Schindele D. Slidling-mode control of a high-speed linear axis driven by pneumatic muscle actuators. IEEE Trans Ind Electron 2008;55:3855-64.

- driver by piecinal indice actions. Item 1208;55:3855-64.

  [36] Danzer MA, Wilhelm J, Aschemann H, Hofer EP. Model-based control of cathode pressure and oxygen excess ratio of a PEM fuel cell system. J Power Source 2008;176:515-22.

  [37] da Silva PSP, Rouchon P, Hatness-based control of a single qubit gate. IEEE Trans Autom Control 2008;53:775-9.

  [38] Song E, Lynch AF, Dinavahi V, Experimental validation of nonlinear control for a voltage source converter. IEEE Trans Control Syst Technol 2009;17:1135-44.

  [39] Rabbani T, Munier S, Dorchies D, Malaterre P, Bayen A, Litrico X. Flatness-based control of open-channel flow in an irrigation canal using SCADA. IEEE Control Syst Mag 2009;29:22-30.

  [40] Gensior A, Sira-Ramirez H, Rudolph J, Guldner H. On some nonlinear current controllers for three-phase boost rectifiers. IEEE Trans Ind Electron 2009;56:360-70.
- 2009;56:360-70.

- 2009:56:360-70.
  [41] Morio V. Cazurang F, Vernis Ph. Flatness-based hypersonic reentry guidance of a lifting-body vehicle. Control Eng Pract 2009:17:588-96.
  [42] Agrawal SK, Pathak K, Franch J, Lampariello R, Hirzinger G. A differentially flat open-chain space robot with arbitrarily oriented joint axes and two momentum wheels at the base. IEEE Trans Autom Control 2009;54:2185-91.
  [43] Fliess M, Lévine J, Martin Ph, Rouchon P. A lie-backlund approach to equivalence and flatness of nonlinear systems. IEEE Trans Autom Control 1000;44:022-27. 99-44-922-37

- 1999:44:922-37.
  [44] Millérioux C, Daafouz J. Flatness of switched linear discrete-time systems. IEEE Trans Autom Control 2009;54:615-9.
  [45] Payman A, Pierfederici S, Meibody-Tabar F, Energy control of supercapacitor/fuel cell hybrid power source. Energy Convers Manage 2008;49:1637-44.
  [46] Liu G, Zhang J, Sun Y, High frequency decoupling strategy for the PEM fuel cell hybrid system. Int J Hydrogen Energy 2008;33:6253-61.
  [47] Rani BI, Aravind CK, Ilango GS, Nagamani C. A three phase PLL with a dynamic feed forward frequency estimator for synchronization of grid connected converters under wide frequency variations. Int J Electr Power Energy Syst 2012;41:63-70. 2012;41:63-70.
- [48] Preitl S, Precup RE. An extension of tuning relations after symmetrical optimum method for PI and PID controllers. Automatica 1999;35(10):1731-6.
   [49] Papadopoulos KG, Margaris NI. Extending the symmetrical optimum criterion to the design of PID type-p control loops. J Process Control 2012;22(1):11-25.

Electrical Power and Energy Systems 65 (2015) 41-48



Contents lists available at ScienceDirect

## **Electrical Power and Energy Systems**

journal homepage: www.elsevier.com/locate/ijepes



## Nonlinear single-loop control of the parallel converters for a fuel cell power source used in DC grid applications



Warit Thammasiriroj <sup>a,\*</sup>, Viboon Chunkag <sup>a</sup>, Matheepot Phattanasak <sup>b</sup>, Serge Pierfederici <sup>c</sup>, Bernard Davat <sup>c</sup>, Phatiphat Thounthong <sup>b</sup>

a Department of Electrical and Computer Engineering, Faculty of Engineering, King Mongkut's University of Technology North Bangkok, Bangkok, Thailand

#### ARTICLE INFO

Article history:
Received 24 October 2013
Received in revised form 9 July 2014
Accepted 4 September 2014
Available online 8 October 2014

Keywords: Fuel cells Interleaved converters Nonlinear control Single-loop feedback control

#### ABSTRACT

This paper presents an innovative control law for a multiphase interleaved converter in the distribution of power supply in fuel cell (FC) generators. Traditionally, to control the DC output power, voltage, or current in a converter, a linear multiple-loop feedback control technique is used. The nonlinear multiple-loop feedback control technique is used. The nonlinear multiple-loop feedback control approach offers several techniques that help to improve the system response. In this paper, an alternative nonlinear single-loop feedback control scheme is proposed. This scheme is based on the differential flatness concept, which provides a solution to achieve the preferred response using a less sophisticated algorithm. To validate the proposed technique, a prototype of a FC power converter (a 600-W two-phase interleaved boost DC-DC converter) was constructed in the laboratory, and the control algorithm was implemented to control the prototype using a dSPACE 1104 controller card. The control scheme exhibited excellent experimental results for use with a 1.2-kW Nexa Ballard polymer electrolyte membrane fuel cell (PEMFC) regarding the steady state and dynamic responses as well as the control robustness.

© 2014 Elsevier Ltd. All rights reserved.

## Introduction

Renewable energy sources are predicted to become competitive with conventional power generation systems in the near future. As shown in Fig. 1, FCs, which play an important role in supporting electricity demand because of their significant advantages of energy efficiency and emission control, normally require a converter to regulate the DC output voltage when applied to variable power loads [1–3].

In such applications, a parallel DC–DC converter shown in Fig. 2 is a competitive option. The DC–DC converter operates under a feedback control to regulate the output voltage and to enable load sharing. This DC–DC converter with closed-loop control is essentially a nonlinear system. However, the common technique used to control the current and voltage in this nonlinear DC–DC converter is the use of two-loop feedback Pl compensators, as shown in Fig. 3(a) (the outer loop is for voltage control and the inner loop is for current control), which is based on linear control theory [4,5].

The subsequent development of nonlinear control techniques, such as the sliding mode control (SMC) and the differential flatness

http://dx.doi.org/10.1016/j.ijepes.2014.09.025 0142-0615/© 2014 Elsevier Ltd. All rights reserved. control approaches shown in Fig. 3(b), has introduced effective means of controlling responses and improving system robustness [6–11]. Multiple-loop feedback control, which is primarily used in complex systems, can increase the sophistication in the design. Two loops are generally required because that is the minimum number of loops required for a set of voltage and current controls.

This paper presents an alternative nonlinear single-loop feedback control based on the differential flatness principle, as shown in Fig. 3(c). This type of feedback control reduces the complexity compared to the common multiple-loop feedback control approach. The most important advantage of the single-loop feedback control is to increase the bandwidth of the feedback control system. The bandwidth of the single-loop feedback control should be limited to about 1/4-1/5 of the switching frequency. On the other hand, the bandwidth of the second loop of the two-loop feedback control should be 1/16-1/25 times of the switching frequency in order to prevent the disturbance, which may impact the stability of the controller [12]. However, the complexity of the single-loop control equations can be easily calculated the duty ratios by a controller. By applying the single-loop feedback control based on the differential flatness concept, the dynamic response of the inductor current and the total static energy changes according to its reference; as a result, the inductor current of any phase is maintained

<sup>&</sup>lt;sup>b</sup> Renewable Energy Research Centre, Department of Teacher Training in Electrical Engineering, King Mongkut's University of Technology North Bangkok, Bangkok 10800, Thailand <sup>c</sup> Groupe de Recherche en Electrotechnique et Electronique de Nancy, Université de Lorraine, 2 avenue de la Forêt de Haye, 54518 Vandoeuvre-les-Nancy, France

<sup>\*</sup> Corresponding author. Tel.: +66 89414 9994; fax: +66 29122070. E-mail address: wrtr@kmutnb.ac.th (W. Thammasiriroj).

W. Thammasiriroj et al./Electrical Power and Energy Systems 65 (2015) 41-48

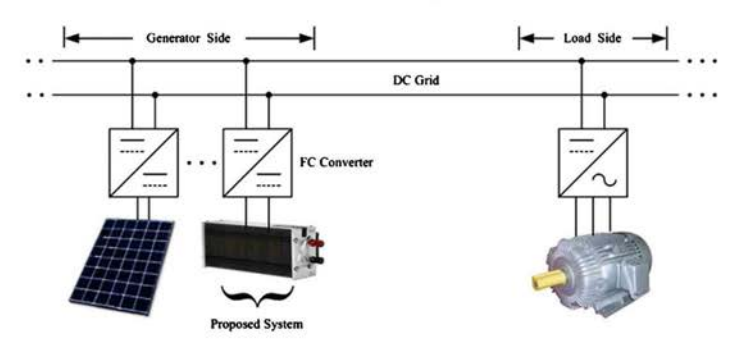


Fig. 1. DC distributed system supplied by renewable energy.

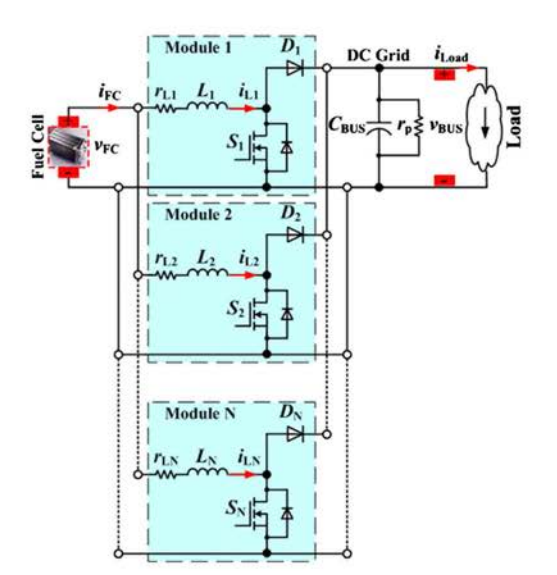


Fig. 2. FC converter: parallel boost converters for FC applications.

by balancing the currents against each other. Moreover, the system is to be controllable and observable under the operation of the differential flatness strategy.

The content of this paper is organized as follows. The structure and model describing the multiphase step-up converter with the parallel switching technique is presented in Section 'Power converter modeling'. A brief introduction to the differential flatness principle and strategies that are used to control the inductor current and the total static energy trajectories are presented in Section 'Control strategy'. The experimental setup and results that validate the proposed control method are described in Section 'Experimental validation'. Finally, the concluding remarks are presented in Section 'Conclusion'.

## Power converter modeling

42

Principally, high-current low-voltage converters are required by reason of the electrical properties of FCs [2,3]. A conventional step-up converter is generally chosen as a FC converter. Nevertheless,

when the power expands the conventional converters will be limited. To overcome this limitation, the utilization of a parallel power converter (multiphase converters in parallel) with an interleaved technique can provide improved performance [9,10]. However, the previous researches [9,10] implemented the converter using a multiple-loop control approach. As a basic principle, the interleaved technique consists of phase shifting the control signals of various converter cells N in parallel [2,7]. The schematic diagram of the proposed multiphase interleaved boost converter for FC applications is shown in Fig. 2. In the case of ideal converters, with the equivalent series and parallel resistances representing losses, the state equation of the converter and the output voltage shown in Fig. 2 are given as:

$$\frac{di_{LK}}{dt} = \frac{1}{L_{V}} [v_{FC} - r_{LK}i_{LK} - (1 - d_K)v_{BUS}] \qquad (1)$$

$$\frac{dv_{BUS}}{dt} = \frac{1}{C_{BUS}} \left[ \sum_{K=1}^{N} (1 - d_K) i_{LK} - \frac{v_{BUS}}{r_P} - i_{Load} \right]$$
(2)

where  $K = \{1,2,3,\ldots,N\}$ ,  $d_R$  is the duty cycle of the pulsewidth modulation (PWM) converter,  $p_{TC}$  is the FC voltage,  $i_{FC}$  is the FC current,  $k_E$  is the input inductance,  $i_{LR}$  is the inductor current in branch K,  $i_{LOad}$  is the load current,  $v_{BLS}$  is the DC bus voltage,  $c_{BLS}$  is the total output capacitance at the DC bus, and  $r_{LK}$  is the series resistance of inductor  $L_K$ . Note that  $r_{LK}$  and  $r_p$  represent the static losses in each boost converter module. The method to obtain these resistances is given in [11].

## Control strategy

## Differential flatness principle

The concept of the differential flatness principle was first introduced by Fliess et al. [13]. This concept allowed an alternate representation of the system involving the use of trajectory planning and nonlinear systems applied across the various implemented engineering concepts, as demonstrated in the following examples: the control of the cathode pressure and the oxygen excess ratio of a PEMFC system [14]; the control of an inverted pendulum and a vertical takeoff and landing in avionic applications [13]; the current control for three-phase three-wire boost converters [15]; and the reactive power and DC output voltage tracking control of a three-phase voltage source converter [16]. Because the flatnessbased control is a model based method, we expect it to have some sensitivity to error in the model parameters. In addition, in [16], the authors demonstrated that the flatness-based control is robust and can provide an improved dynamic tracking performance relative to a classical linear control technique (e.g., a Pl controller).

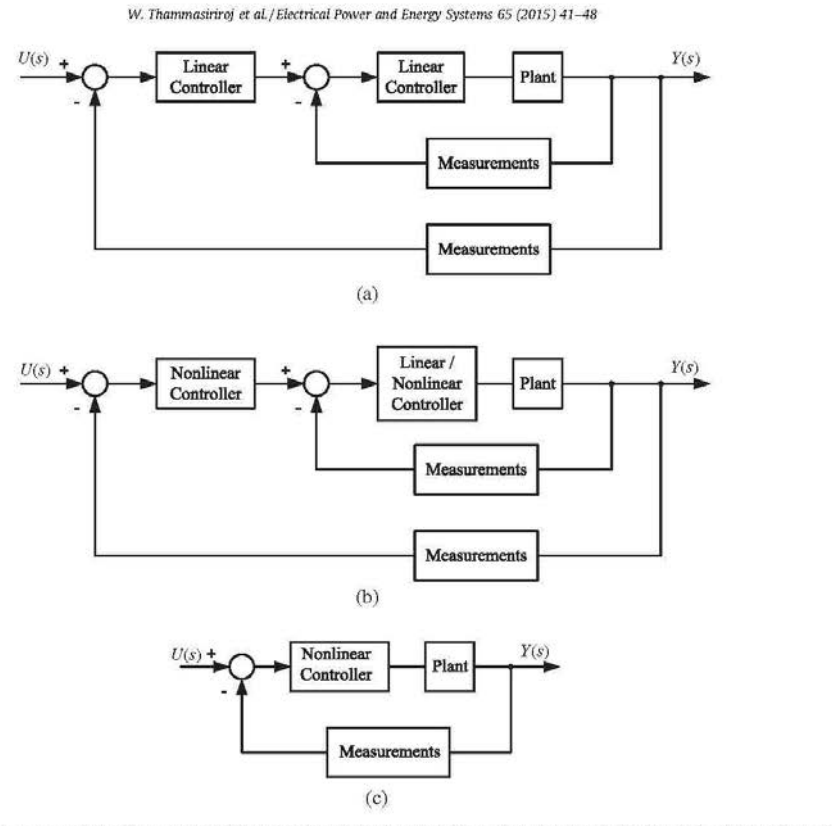


Fig. 3. Control structures for a power electronics converter: (a) linear two-loop feedback control, (b) nonlinear two-loop feedback control, and (c) nonlinear single-loop feedback control.

Briefly, a nonlinear system is flat [17–18] if there exists a set of differentially independent variables (equal in number to the number of inputs) such that all state variables  $\mathbf{x}$  and flat input variables  $\mathbf{u}$  can be expressed in terms of those flat output variables  $\mathbf{y}$  and a finite number of their time derivatives without integrating the differential equations [13]. Especially, the system is flat if the system has state variables  $\mathbf{x} \in \mathfrak{R}^n$ , flat input variables  $\mathbf{u} \in \mathfrak{R}^n$ , and flat output variables  $\mathbf{y} \in \mathfrak{R}^m$  that can be found of the form [13]:

$$\mathbf{y} = \phi(\mathbf{x}, \mathbf{u}, \dot{\mathbf{u}}, \dots, \mathbf{u}^{(\alpha)}) \tag{3}$$

such that

$$\mathbf{x} = \varphi(\mathbf{y}, \dot{\mathbf{y}}, \dots, \mathbf{y}^{(\beta)}) \tag{4}$$

$$\mathbf{u} = \psi(y, \dot{y}, \dots, y^{(\beta+1)}) \tag{5}$$

with  $rank(\phi) = m$ ,  $rank(\psi) = m$ , and  $rank(\phi) = n$ .

Flatness of the power converters

To control the energy in the system, the total static energy of the system is defined as a flat output  $y_T$ , which can be expressed as:

$$y_{\rm T} = \sum_{\rm K=1}^{\rm N} \frac{1}{2} L_{\rm K} i_{\rm LK}^2 + \frac{1}{2} C_{\rm BUS} v_{\rm BUS}^2 \tag{6}$$

From (1) and (2), if we assume the losses of the system become zero  $(r_{LR}=0 \text{ and } r_p\approx \infty)$  and substitute into (6), the first and second order differential equations of  $y_T$  can be written as:

$$\dot{y}_{\rm T} = \nu_{\rm FC} \sum_{\rm LK}^{\rm N} i_{\rm LK} - \nu_{\rm BUS} i_{\rm Load} \tag{7}$$

$$\ddot{y}_{\rm T} = \nu_{\rm FC}^2 \left( \sum_{K=1}^{N} \frac{1}{L_{\rm K}} \right) - \nu_{\rm FC} \nu_{\rm BUS} \left( \sum_{K=1}^{N} \frac{1 - d_{\rm k}}{L_{\rm K}} \right)$$
(8)

Therefore, the state variable  $v_{\mathrm{BUS}}$  can be given by

$$\nu_{\text{BUS}} = \phi(\mathbf{i}_{\text{LK}}, \mathbf{y}_{\text{T}}, \dot{\mathbf{y}}_{\text{T}}, \ddot{\mathbf{y}}_{\text{T}}) \tag{9}$$

where  $i_{\rm Load}$  is a function of  $v_{\rm BUS}$ , and  $v_{\rm FC}$  is approximately constant compared with the other variables.

To control the inductor current balance between the converters, we assume  $i_{L1}$  to be a reference inductor current and define another flat output variable  $y_{K}$ :

$$y_{K} = i_{L1} - i_{LK}, \quad \forall K \in \{2, \dots, N\}$$
 (10)

For this system, we choose the flat output vector from (6) and (10):

$$\mathbf{y} = [y_{\mathsf{T}}, y_{\mathsf{2}}, \dots, y_{\mathsf{N}}]^{\mathsf{T}} \tag{11}$$

Then, we define the state variables x as follows:

$$\mathbf{X} = [i_{L1}, i_{L2}, \dots, i_{LN}, \nu_{BUS}]^{T}$$
(12)

The summation of all the inductor currents is the FC current:

$$i_{PC} = i_{L1} + i_{L2} + \ldots + i_{LN}$$
 (13)

W. Thammasiriroj et al./Electrical Power and Energy Systems 65 (2015) 41-48

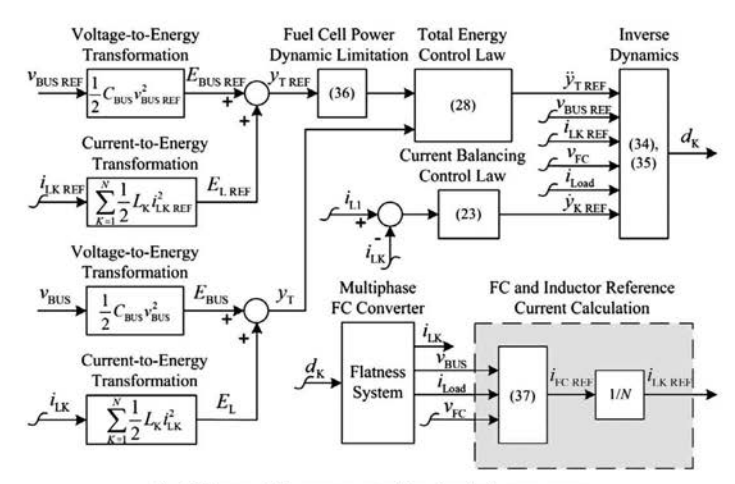


Fig. 4. Diagram of FC converter control based on the flatness concept.

Eq. (13) can be rearranged in the following form:

$$i_{FC} = i_{L1} + \sum_{k=2}^{N} i_{LK}$$
 (14)

By using (10), (13) and (14), one can deduce the inductor current  $i_{L1}$ , which is in a function of flat outputs:

$$i_{L1} = \frac{1}{N} \left( i_{FC} + \sum_{K=2}^{N} y_K \right) = \varphi(y_K)$$
 (15)

The differential equation of (10) can be expressed as:

$$\dot{y}_{K} = \frac{di_{L1}}{dt} - \frac{di_{LK}}{dt}, \quad \forall K \in \{2, \dots, N\}$$
 (16)

The results from (6)-(16) can be summarized as follows:

$$i_{LK} = \varphi(y_K, \dot{y}_K, y_T, \dot{y}_T, \ddot{y}_T), \quad \forall K \in \{1, ..., N\}$$
 (17)

$$\nu_{\text{BUS}} = \varphi(y_{\text{K}} \, \dot{y}_{\text{K}} \, y_{\text{T}} \, \dot{y}_{\text{T}} \, \ddot{y}_{\text{T}}) \tag{18}$$

$$\mathbf{x} = \left[\mathbf{i}_{\text{L1}}, \mathbf{i}_{\text{L2}}, \dots, \mathbf{i}_{\text{LN}}, \nu_{\text{BUS}}\right]^T = \phi(\mathbf{y}_{\text{K}}, \dot{\mathbf{y}}_{\text{K}}, \mathbf{y}_{\text{T}}, \dot{\mathbf{y}}_{\text{T}}, \ddot{\mathbf{y}}_{\text{T}}) \tag{19}$$

In this study, a two-phase interleaved converter is chosen to implement the system because of the limitation of the inputs and outputs of the dSPACE DS1104 controller card. Therefore, N=2 is selected to validate the control algorithm because the two-phase converter is sufficient to verify the innovative control scheme. Using (1), (2), (8) and (16) and neglecting the resistive losses, the input variables of the flatness control can be expressed by:

$$\begin{split} d_1 &= \frac{1}{\left(L_1 i_{L1} + L_2 i_{L2} + \frac{C_{BUS} \nu_{BUS} \nu_{FC}}{i_{Iood}}\right)} \left[L_1 \nu_{BUS}^2 \left(-i_{Load} + i_{L1} + i_{L2} + \frac{L_2 i_{L2} \dot{y}_2}{\nu_{FC}}\right) \\ &+ \frac{L_1 C_{BUS} \nu_{BUS}^2}{2 i_{Load}} \left(-\frac{i_{L1}}{i_{Load}} - \frac{i_{L2}}{i_{Load}} + \frac{\nu_{FC}}{L_1} + \frac{\nu_{FC}}{L_2} + \dot{y}_2 + \frac{\ddot{y}_T}{\nu_{BUS}}\right)\right] \end{split} \tag{20}$$

$$\begin{split} d_{2} &= \frac{1}{\left(L_{1}\dot{i}_{L1} + L_{2}\dot{i}_{L2} + \frac{c_{\text{BUS}}v_{\text{BUS}}v_{\text{FC}}}{i_{\text{load}}}\right)} \Bigg[L_{2}\,v_{\text{BUS}}^{2} \bigg(-i_{\text{Load}} + i_{L1} + i_{L2} - \frac{L_{1}\dot{i}_{L1}\dot{y}_{2}}{v_{\text{FC}}}\bigg) \\ &+ \frac{L_{2}c_{\text{BUS}}\,v_{\text{BUS}}^{2}}{2i_{\text{Load}}} \bigg(-\frac{i_{L1}}{i_{\text{Load}}} - \frac{i_{L2}}{i_{\text{Load}}} + \frac{v_{\text{FC}}}{L_{1}} + \frac{v_{\text{FC}}}{L_{2}} - \dot{y}_{2} + \frac{\ddot{y}_{\text{T}}}{v_{\text{BUS}}}\bigg)\Bigg] \end{split} \tag{21}$$

$$\mathbf{u} = [d_1 d_2]^T = \psi(y_K, \dot{y}_K, y_T, \dot{y}_T, \ddot{y}_T)$$
 (22)

Table 1 Converter parameters and semiconductor devices.

Devices	Specification	
Inductors: $L_1$ and $L_2$	1.85 mH and 1.80 mH	
Output capacitor: CBUS	1,360 μF	
MOSFETs: S <sub>1</sub> and S <sub>2</sub>	IRFP264N: 38 A, 250 V	
Diodes: D <sub>1</sub> and D <sub>2</sub>	RURG3020: 30 A, 200 V	

By using (19) and (22), this system can express all the state variables and input variables in terms of the flat output and a finite number of its derivatives, which are the properties of the flat system. Therefore, we can conclude that this is a flat system.

Control laws

First, the desired reference trajectory is the inductor current reference trajectory  $y_{\rm K}$  Ref. A linear close-loop control law earning an exponential asymptotic error tracking  $y_{\rm K}-y_{\rm K}$  Ref of the trajectory is expressed by the following equation.

$$(\dot{y}_{K} - \dot{y}_{K \text{ REF}}) + \lambda_{K1}(y_{K} - y_{K \text{ REF}}) + \lambda_{K2} \int (y_{K} - y_{K \text{ REF}}) d\tau = 0$$
 (23)

Then, we determine  $e_K = y_K - y_{K \text{ REF}}$ , which leads to

$$\ddot{e}_{K} + \lambda_{K1}\dot{e}_{K} + \lambda_{K2}e_{K} = 0 \tag{24}$$

An optimum choice of the design controller parameters is obtained by matching the characteristic polynomial  $c_R(s)$  to a desired characteristic polynomial with defined root locations.

The desired characteristic equation and controller parameters

$$c_{\mathbf{K}}(s) = s^2 + 2\zeta_{\mathbf{K}}\omega_{\mathbf{K}}s + \omega_{\mathbf{K}}^2 \tag{25}$$

$$\lambda_{K1} = 2\zeta_K \omega_K \tag{26}$$

$$\lambda_{K2} = \omega_K^2 \tag{27}$$

where  $\varpi_{\rm K}$  and  $\zeta_{\rm K}$  are the natural frequency and the desired dominant damping ratio, respectively.

Obviously, the control system is stable for  $\lambda_{K1}$ ,  $\lambda_{K2} > 0$  ( $\zeta_{K}$ ,  $\omega_{K} > 0$ ). Fig. 4 depicted the proposed control law of the inductor currents detailed above.

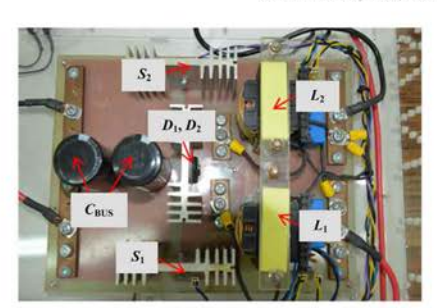


Fig. 5. Prototype of the two-phase parallel boost converter.

Second, the desired reference trajectory is the total energy reference trajectory  $y_{\rm T~REF}$ . The following equation expresses a linear closed-loop control law achieving an asymptotic error tracking  $y_{\rm T}-y_{\rm T~REF}$  of the trajectory.

$$\begin{split} &(\ddot{y}_T - \ddot{y}_{T\,REF}) + \lambda_{T1}(\dot{y}_T - \dot{y}_{T\,REF}) + \lambda_{T2}(y_T - y_{T\,REF}) \\ &+ \lambda_{T3} \int (y_T - y_{T\,REF}) d\tau = 0 \end{split} \tag{28}$$

where the set of controller parameters  $(\lambda_{T1},\lambda_{T2} \text{ and } \lambda_{T3})$  is chosen. If we define  $e_T$  =  $y_T$  –  $y_T$   $_{REF}$ , we obtain

$$e_T + \lambda_{T1}\ddot{e}_T + \lambda_{T2}\dot{e}_T + \lambda_{T3}e_T = 0 \tag{29}$$

As mentioned earlier, a desired characteristic polynomial  $c_{\rm T}(s)$  is optimized by the designed root locations. The desired characteristic equation and controller parameters are expressed as:

$$c_{T}(s) = (s+p)(s^{2} + 2\zeta_{T}\omega_{T}s + \omega_{T}^{2})$$
 (30)

$$\lambda_{T1} = 2\zeta_T \omega_T + p \tag{31}$$

$$\lambda_{T2} = 2\zeta_T \omega_T p + \omega_T^2 \tag{32}$$

$$\lambda_{T3} = \omega_T^2 p \tag{33}$$

where  $\zeta_T$ ,  $\omega_T$  and p are the desired damping ratio, angular frequency and pole of the compensator, respectively. By using this control law, the DC bus voltage always tracks its reference.

To control the system using differential flatness properties, the calculated references are replaced into their measured values to calculate the duty cycles in (20) and (21). The duty cycles  $d_1$  and  $d_2$  are therefore expressed by:

$$\begin{split} d_{1} &= \frac{1}{\left((L_{1} + L_{2})i_{1K\,REF} + \frac{C_{NCLPINS,\,REF}P_{IY}}{load}\right)} \left[L_{1}\nu_{BUS\,REF}^{2}\left(-i_{Load} + 2i_{LK\,REF} + \frac{L_{2}i_{LK}\dot{y}_{2REF}}{\nu_{FC}}\right) \right. \\ &\left. + \frac{L_{1}C_{BUS}\,\nu_{BUS\,REF}^{2}\left(-\frac{2i_{LK}}{i_{Load}} + \frac{\nu_{FC}}{L_{1}} + \frac{\nu_{FC}}{L_{2}} + \dot{y}_{2REF} + \frac{\ddot{y}_{T\,REF}}{\nu_{BUS\,REF}}\right)\right] \end{split} \tag{34} \end{split}$$

$$\begin{aligned} d_2 &= \frac{1}{\left((L_1 + L_2)i_{\text{ILK REF}} + \frac{C_{\text{BIC}}\nu_{\text{BUS}}}{i_{\text{tod}}}\right)} \left[L_2 \nu_{\text{BUS REF}}^2 \left(-i_{\text{Load}} + 2i_{\text{ILK REF}} - \frac{L_1 i_{\text{ILK}} j_{\text{ZREF}}}{\nu_{\text{PC}}}\right) \right. \\ &\left. + \frac{L_2 C_{\text{BUS}} \nu_{\text{BUS}}^2 REF}{2i_{\text{Load}}} \left(-\frac{2i_{\text{LK}}}{i_{\text{Load}}} + \frac{\nu_{\text{FC}}}{L_1} + \frac{\nu_{\text{FC}}}{L_2} - \dot{y}_{\text{ZREF}} + \frac{\ddot{y}_{\text{T} \text{REF}}}{\nu_{\text{BUS REF}}}\right)\right] \end{aligned}$$
(35)

Even though, the duty cycles shown in (34) and (35) seem to be more complicated than the results of the classical multiple-loop strategies, the duty cycles can be easily substituted and calculated by a controller. However, the single-loop control can reduce the design complexity of the multiple-loop ones by the systematic design as shown before.

Finally, the FC power dynamic limitation enables safe operation of the FC [9]. To obtain a linear transfer function, a second-order filter  $G_F(s)$  is selected for controlling the FC power dynamics.

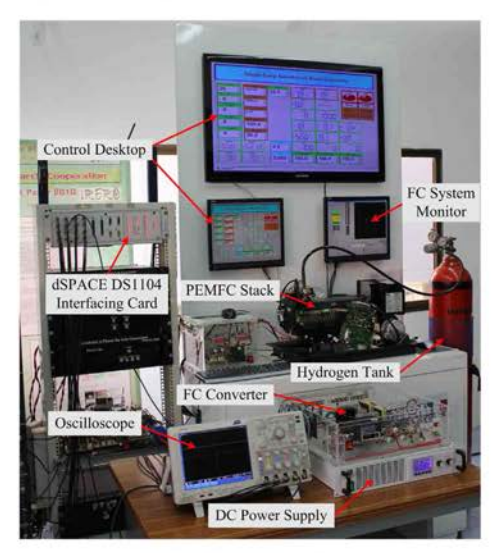


Fig. 6. System test bench.

Table 2
Flatness control and dynamic limitation parameters.

Parameters	Descriptions	Values
ζ <sub>2</sub>	Damping ratio of $c_2(s)$	1
$\omega_2$	Natural frequency of $c_2(s)$	157 rad s-1
ζ <sub>T</sub>	Damping ratio of $c_T(s)$	1
$\omega_{\text{T}}$	Natural frequency of $c_{1}(s)$	314 rad s
p	Desired pole of $c_T(s)$	628 rad s-1
ζ <sub>F</sub>	Damping ratio of $G_F(s)$	1
Ω <sub>E</sub>	Natural frequency of $G_F(s)$	0.4 rad s-1

$$G_{F}(s) = \frac{1}{\left(\frac{s}{c_{c_{c_{c}}}}\right)^{2} + \frac{2\zeta_{F}}{c_{c_{c_{c}}}}s + 1}$$
(36)

where  $\omega_{\rm F}$  and  $\zeta_{\rm F}$  are the regulation parameters.

In addition, the reference of the FC current  $i_{\rm FC\ REF}$  and the inductor current  $i_{\rm LK\ REF}$  can approximately be expressed by

$$i_{FC REF} = \frac{v_{Bus} i_{Load}}{v_{FC} - \sum_{k=1}^{N} \frac{1}{k-1}}$$
(37)

$$i_{\text{LK REF}} = \frac{i_{\text{FC REF}}}{N} \tag{38}$$

## **Experimental validation**

Description of the test bench

The parameters of the two-phase interleaved converter are detailed in Table 1 and portrayed in Fig. 5. A small-scale test bench as illustrated in Fig. 6 was implemented in the laboratory. The PEMFC system (a Nexa Ballard PEMFC power generator: 1.2 kW, 26 V, 46 A) was used as the DC power supply of the system to test the system characteristics and determine the steady state behaviors. A separate constant DC power supply was used to test the transient response and control system robustness. The feedback control loop detailed in Fig. 4 was implemented through the



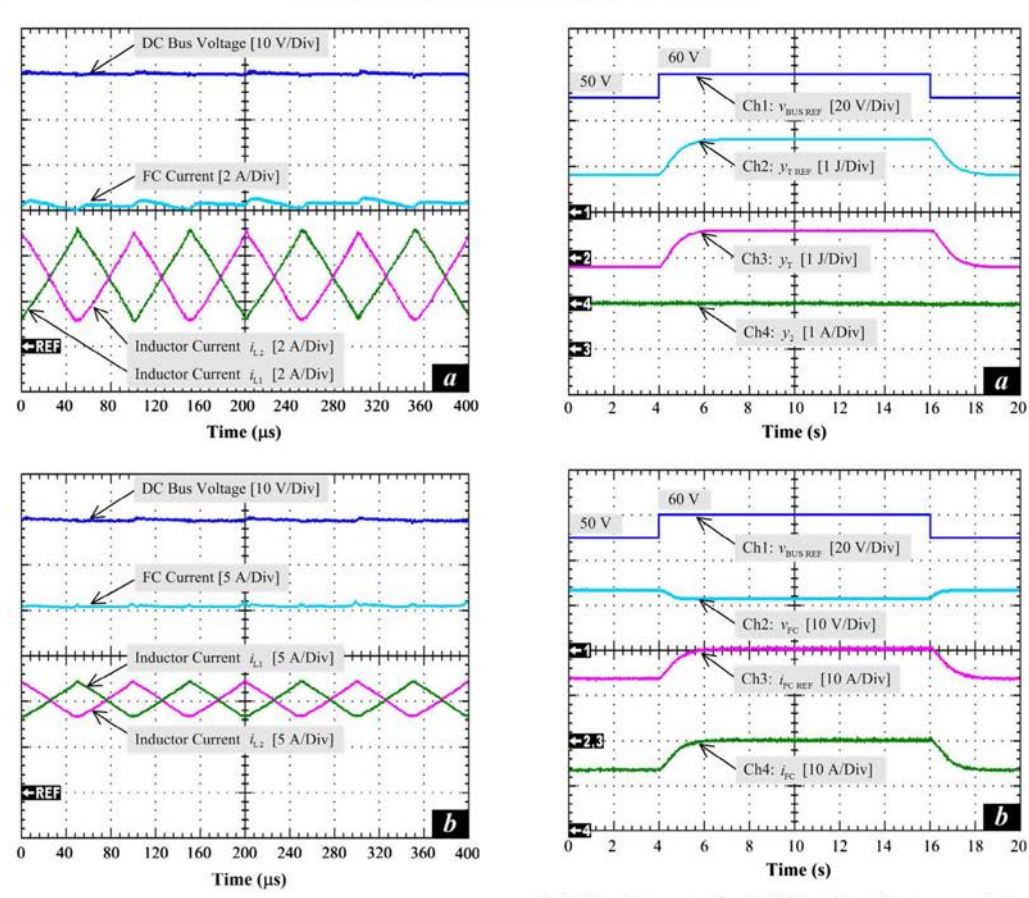


Fig. 7. Steady-state characteristics of the converter at the load powers of (a) 200 W, and (b)  $600\,W$ .

**Fig. 8.** Dynamic responses when the DC bus voltage reference  $v_{\text{BUS REF}}$  is changed from 50 V to 60 V at t=4 s and from 60 V to 50 V at t=16 s. (a) Flat output variable and its reference. (b) FC voltage and current and its reference.

controller card dSPACE DS1104 platform as shown in Fig. 6. The converter operated at a switching frequency of 10 kHz. The nonlinear controller parameters used for controlling the system energy and balancing the inductor currents are listed in Table 2.

## Experimental results

(1) Steady state test using the FC converter supplied by a PEMFC:
The experimental waveforms in Fig. 7 describe the steadystate responses of the interleaved converters at the output
power reference of 200 W in Fig. 7(a) and 600 W in
Fig. 7(b). Summation of the two inductor currents resulted
in the FC current exhibiting lower current ripple compared
to its original inductor currents. This result highlights the
advantage of multiphase DC-DC converters. The upper trace
displays the output DC voltage that met the set point of 60 V.
Note that the two phases of the inductor current shared an
equal average current value with the out-of-phase waveforms. Moreover, these two phase current waveforms cancel
each other and thus reduce the FC input-ripple current
caused by the interleaved switching technique. It should

be note that if the output power level decreases the converter may go into discontinuous conduction mode (DCM). To avoid DCM, the converter must have bidirectional capability by replacing the output diodes with controlled switches. However, it is beyond this paper.

(2) Dynamic performance test using the FC converter supplied by a PEMFC: As shown in Fig. 8, the test started with the DC bus voltage reference of 50 V (Ch1). Subsequently, at t = 4 s it was stepped up to 60 V and remained for 12 s before stepping back to 50 V thereafter. In Fig. 8(a), Ch2 and Ch3, which represents the total static energy reference and measured total static energy, respectively, exhibited a good result of the tracking system. Likewise, in Fig. 8(b), Ch3 and Ch4, which represents the FC current and its reference, were both in phase; as a result, the flat output y<sub>2</sub> [Ch4 in Fig. 8(a)] is nearly zero. Therefore, the response of the inductor currents in the converter verified the highly controlled response using the flatness properties with only one loop control structure. However, Ch4 in Fig. 8(b) shows a variation of the FC current depending on the output voltage because the resistive load was constant during the experimentation.

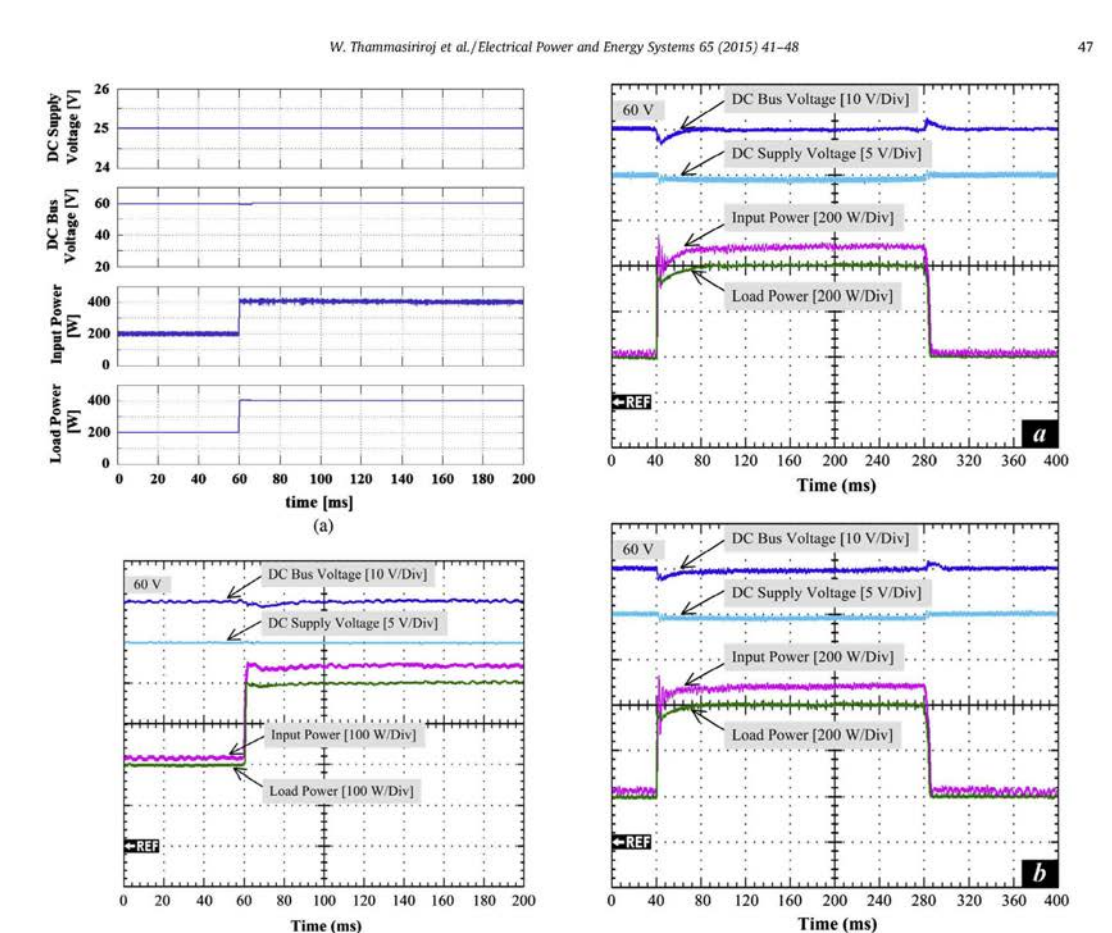


**Fig. 9.** The dynamic characteristics of the power converter during a step load change from  $200\,\mathrm{W}$  to  $400\,\mathrm{W}$  at  $t = 60\,\mathrm{ms}$ . (a) Simulation wavesforms. (b) Experimental waveforms.

Time (ms) (b)

**Fig. 10.** Comparison of the DC bus voltage regulation (DC link stabilization) of the power plant during a large load step. (a) Exact model  $(r_{L1}=0.10~\Omega,~r_{L2}=0.12~\Omega,~r_p=250~\Omega)$ . (b) Error model (robustness)  $(r_{L1}=r_{L2}=0~\Omega$  and  $r_p\approx\infty~\Omega)$ .

(3) Control robustness test using the FC converter supplied by a DC power supply: Because the FC generator has slow dynamics by nature, it is dangerous to perform dynamic testing on an FC stack [19–22]. Therefore, instead of a FC, this dynamic testing was supplied by a 25-V DC power supply. The simulation and oscilloscope waveforms in Fig. 9(a) and (b) shows the dynamic response of the dc bus voltage dynamics to the load power demands (disturbance) from 200 W to 400 W. The proposed controller demonstrates good stability and an optimum response (no oscillation and a short settling time) for the regulation of the dc bus voltage to the desired reference of 60 V.

To substantiate the robustness and dynamic regulation of the dc-bus voltage using the proposed control scheme, Fig. 10 illustrates waveforms that were obtained during the presence of a large load step. Using the exact model resulted in the rapid response in the output voltage loop to reject the perturbation. Despite the errors in the converter model, the system was still able to function, and the waveforms obtained in Fig. 10(a) were quite similar to

those measured in Fig. 10(b). The DC bus voltage ripple swing could be easily improved by increasing either the capacitance  $C_{\rm BUS}$  or the angular frequency.

This paper profoundly presents the concept and experiments of the single-loop control. However, the multiple-loop control was previously presented in the reference [9]. Additionally, the dynamic response of this strategy (switching frequency = 10 kHz) is faster than the experimental results shown in the reference (switching frequency = 25 kHz) as the reason explained before.

## Conclusion

In this paper, a nonlinear single-loop feedback control scheme based on the differential flatness concept was proposed for use in a multiphase parallel converter. This scheme offers an alternative solution that reduces the sophistication of the algorithm design while effectively achieving the preferred response. Validation of the proposed scheme was achieved by demonstrating control of a prototype set of a fuel cell stack with a 600-W two-phase boost converter connected in parallel, which was implemented through

W. Thammasiriroj et al./Electrical Power and Energy Systems 65 (2015) 41-48

a dSPACE 1104 controller card. Three aspects of the control scheme  $\,$ were verified, including steady state response, dynamic response, and control robustness. The experiments exhibited overall good results, which implied that this designed scheme has the potential to be applied in FC generator applications, as well as in a hybrid power source system, such as hybrid electric vehicles.

#### Acknowledgments

This work was supported in part by the research program in cooperation with the Thai-French Innovation Institute (TFII), King Mongkut's University of Technology North Bangkok (KMUTNB) with Université de Lorraine, in part by the Energy Conservation Promotion Fund under Grant 049/2556 and in part by the Thailand Research Fund (TRF) and Faculty of Technical Education (Research Grant for Mid-Career University Faculty) under Grant RSA5580009.

- Dursun E, Kilic O. Comparative evaluation of different power management strategies of a stand-alone PV/Wind/PEMFC hybrid power system. Int J Electr Power Energy Syst 2012;34:81–9.

   Thounthong P, Tricoli P, Davat B. Performance investigation of linear and nonlinear controls for a fuel cell/supercapacitor hybrid power plant. Int J Electr Power Energy Syst 2014;54:454–64.

   Hajizadeh A, Golkar MA. Control of hybrid fuel cell/energy storage distributed generation system against voltage sag. Int J Electr Power Energy Syst 2010;32:488–97.

   Ramasamy M. Thangavel S. Photovoltaic based dynamic voltage restorer with
- [4] Ramasamy M, Thangavel S. Photovoltaic based dynamic voltage restorer with ower saver capability using PI controller. Int J Electr Power Energy Syst
- 2012;36:51-9.
   Mahery HM, Babaei E. Mathematical modeling of buck-boost dc-dc converter and investigation of converter elements on transient and steady state responses. Int J Electr Power Energy Syst 2013;44:949-63.
   Chen Z. P. Pl and sliding mode control of a Cuk converter. IEEE Trans Power Electron 2012;27(8):3695-703.
- [7] Giral R, Calvente J, Utkin VI, Martinez-Salamero L. Interleaved converters based on sliding-mode control in a ring configuration. IEEE Trans Circuits Syst 1 Reg Papers 2011;58(10):2566-77.

- [8] Thammasiriroj W, Nuchkrua T, Ruayariyasub S. Sliding mode control for stabilizing DC-link of DC-DC converter in photovoltaic systems. Proc PEDG 2010;347–51.
  [9] Thounthong P, Pierfederici S. A new control law based on the differential flatness principle for multiphase interleaved DC-DC converter. IEEE Trans Circuits Syst II Exp Brief 2010;57(11):903–7.
  [10] Payman A, Pierfederici S. Meibody-Tabar F. Energy management in a fuel cell/supercapacitor multisource/multiload electrical hybrid system. IEEE Trans Power Electron 2009;24(12):2681–91.
  [11] Zandi M, Gavagsaz R, Phattanasak M, Martin JP, Nahidmobarakeh B, Pierfederici S, et al. Flatness based control of a non-ideal DC/DC boost converter. Proc IECON 2011;1360–5.
  [12] Middlebrook RD. Topics in multiple-loop regulators and current-mode programming. IEEE Trans Power Electron 1987;PE-2(2):109–24.
  [13] Fliess M, Lévine J, Martin Ph, Rouchon P. Flatness and defect of non-linear systems: introductory theory and examples. Int J Cont. 1995;61(6):1327–61.
  [14] Danzer MA, Wilhelm J, Aschemann H, Hofer EP. Model-based control of cathode pressure and oxygen excess ratio of a PEM fuel cell system. J Power Sources 2008;176(2):515–22.
  [15] Gensior A, Sira-Ramirez H, Rudolph J, Guldner H, On some nonlinear current.

- (15) Gension A. Sira-British I. Sudolph J. Guldner H. On some nonlinear current controllers for three-phase boost rectifiers. IEEE Trans Ind Electron 2009;56(2):360-70.
  [16] Song E. Lynch Af, Dinavahi V. Experimental validation of nonlinear control for a voltage source converter. IEEE Trans Control Syst Technol 2009;17(5):1135-44.
  [17] Rabbani T, Munier S, Dorchies D, Malaterre P, Bayen A, Litrico X. Flatness-based control of open-channel flow in an irrigation canal using SCADA. IEEE Control Syst Mag 2009;29(5):22-30.
  [18] Agrawal SK, Pathak K, Franch J, Lampariello R, Hizzinger G. A differentially flat open-chain space robot with arbitrarily oriented joint axes and two momentum wheels at the base. IEEE Trans Autom Control 2009;54(9):2185-91.
  [19] Thounthong P, Davat B, Raël S, Sethakul P, Fuel starvation: analysis of a DEM.
- 2009;54(9):2185-91. 19] Thounthong P, Davat B, Raël S, Sethakul P, Fuel starvation: analysis of a PEM fuel cell system. IEEE Ind Appl Mag 2009;15(4):52-9. [20] Thounthong P, Pierfederici S, Davat B. Analysis of differential flatness-based control for a fuel cell hybrid power source. IEEE Trans Energy Convers
- 2010; 25(3):909-20.
  [21] Zhu GR, Loo KH, Lai YM, Tse CK. Quasi-maximum efficiency point tracking for
- [21] Zhu GiK, Loo KH, Lai YM, Ise C.K. Quasi-maximum efficiency point tracking for direct methanol fuel cell in DMF(Supercapacitor hybrid energy system. IEEE Trans Energy Convers 2012;27(3):561–71.
   [22] Haruni AMO, Negnevitsky M, Haque MdE, Gargoom A. A novel operation and control strategy for a standalone hybrid renewable power system. IEEE Trans Sustain Energy 2013;4(2):402–13.

Elsevier Editorial System(tm) for Transportation Research Part C Manuscript Draft

Manuscript Number: TRC-D-14-00410

Title: Energy Management of a Ground Isolated Magnetic Coupling Converter for Supercapacitor Based Transportation Applications

Article Type: Research Paper

Keywords: Converters; energy management; nonlinear systems; supercapacitors; transportation; vehicles.

Corresponding Author: Dr. Phatiphat Thounthong,

Corresponding Author's Institution: King Mongkut's University of Technology North Bangkok

First Author: Phatiphat Thounthong

Order of Authors: Phatiphat Thounthong; Matheepot Phattanasak, PhD; Pietro Tricoli, PhD; Jean-Philippe Martin, PhD; Serge Pierfederici, PhD; Bernard Davat, PhD

Abstract: This paper presents a new energy control algorithm for dc-grid stabilization in weak transportation networks that employ supercapacitors as the energy storage unit. For safety reason and higher voltage conversion gain, a ground isolated converter based on a dual active bridge topology is presented. Using a nonlinear control approach based on the flatness property, we propose a simple solution to dynamic and stabilization problems in the power electronics systems of transportation networks. Furthermore, high dynamics in the disturbance rejection are achieved, which is the key contribution described in this paper. To validate the proposed method, a hardware system is modeled using digital estimation with a DS1103 dSPACE controller platform. We analyze a prototype small-scale network that uses a 1 kW six-pulse rectifier as a dc main station and a 250 F, 32 V supercapacitor bank as an energy storage substation. Finally, the utility of the control algorithm is validated using experimental results measured during motoring mode, ride-though, and braking mode drive cycles.

Suggested Reviewers: Petar Grbović PhD HUAWEI TECHNOLOGIES Duesseldorf GmbH petar.grbovic@ge.com; pgrbovic@yahoo.com He is specialize on Supercapacitor.

Alfred Rufer PhD Professor, École polytechnique fédérale de Lausanne alfred.rufer@epfl.ch He is specialize on supercapacitor and power electronics.

Luigi Piegari PhD Assoc. Prof., Department of Electrical Engineering, Politecnico di Milano luigi.piegari@polimi.it He is specialize on power electronics applications and storage devices.

Álvaro López-López PhD

\*Manuscript
Click here to view linked References

TRANSPORTATION RESEARCH PART C: EMERGING TECHNOLOGIES. | 1

## Energy Management of a Ground Isolated Magnetic Coupling Converter for Supercapacitor Based Transportation Applications

Phatiphat Thounthong<sup>a,w</sup>, Matheepot Phattanasak<sup>a</sup>, Pietro Tricoli<sup>b</sup>

Jean-Philippe Martin<sup>c</sup>, Serge Pierfederici<sup>c</sup>, and Bernard Davat<sup>c</sup>

<sup>a</sup>Renewable Energy Research Centre, Department of Teacher Training in Electrical Engineering, Faculty of Technical Education, King Mongkut's University of Technology North Bangkok 1518, Pracharat 1 Road, Wongsawang, Bangsue, Bangkok 10800, Thailand

> <sup>b</sup>School of Electronic, Electrical and Computer Engineering University of Birmingham Gisbert Kapp Building - B15 2TT, Birmingham, United Kingdom

<sup>c</sup>Groupe de Recherche en Electrotechnique et Electronique de Nancy, Université de Lorraine 2, Avenue de la Forêt de Haye, Vandœuvre-lés-Nancy, Lorraine 54516, France

\*Corresponding Author. Tel.: +66 2 913 2500x3332, fax: +66 2 587 8255. E-mail: phtt@kmutnb.ac.th

## ABSTRACT

This paper presents a new energy control algorithm for dc-grid stabilization in weak transportation networks that employ supercapacitors as the energy storage unit. For safety reason and higher voltage conversion gain, a ground isolated converter based on a dual active bridge topology is presented. Using a nonlinear control approach based on the flatness property, we propose a simple solution to dynamic and stabilization problems in the power electronics systems of transportation networks. Furthermore, high dynamics in the disturbance rejection are achieved, which is the key contribution described in this paper. To validate the proposed method, a hardware system is modeled using digital estimation with a DS1103 dSPACE controller platform. We analyze a